Journal of Food and Drug Analysis

Volume 32 | Issue 3 Article 4

Unlocking early detection of Alzheimer's Disease: The emerging role of nanomaterial-based optical sensors

REVIEW ARTICLE

Unlocking early detection of Alzheimer's disease: The emerging role of nanomaterial-based optical sensors

Chun-Hsien Chen [a,1], Hsin-Hua Liang [b,e,f,1], Chun-Chi Wang [a,c,d], Yi-Ting Yang [e], Yi-Hui Lin [b,*], Yen-Ling Chen [a,e,f,g,**]

[a] School of Pharmacy, College of Pharmacy, Kaohsiung Medical University, Kaohsiung 807378, Taiwan
[b] School of Pharmacy, China Medical University, Taichung 406040, Taiwan
[c] Drug Development and Value Creation Research Center, Kaohsiung Medical University, Kaohsiung 807378, Taiwan
[d] Department of Medical Research, Kaohsiung Medical University Hospital, Kaohsiung 807378, Taiwan
[e] Department of Chemistry and Biochemistry, National Chung Cheng University, Chia-Yi 621301, Taiwan
[f] Center for Nano Bio-Detection, National Chung Cheng University, Chiayi 621301, Taiwan
[g] Department of Fragrance and Cosmetic Science, College of Pharmacy, Kaohsiung Medical University, Kaohsiung 807378, Taiwan

Abstract

Alzheimer's disease (AD) is a chronic and progressive neurodegenerative disorder that affects millions of individuals worldwide. Researchers have conducted numerous studies to find accurate biomarkers for early AD diagnosis and develop more effective treatments. The main pathological hallmarks of AD are amyloid beta and Tau proteins. Other biomarkers, such as DNA, RNA, and proteins, can also be helpful in early AD diagnosis. To diagnose and treat AD promptly, it is essential to accurately measure the concentration of biomarkers in the cerebrospinal fluid or blood. However, due to the low concentrations of these biomarkers in the body, highly sensitive analytical techniques are required. To date, sensors have become increasingly important due to their high sensitivity, swift detection, and adaptable manipulation features. These qualities make them an excellent substitute for conventional instruments. Nanomaterials are commonly employed in sensors to amplify signals and improve sensitivity. This review paper summarized the integration of nanomaterials in optical sensor systems, including colorimetric, fluorescent, and surface-enhanced Raman scattering sensors for AD biomarkers detection.

Keywords: Alzheimer's disease, Biomarkers, Nanomaterials, Optical sensors

1. Alzheimer's disease

Alzheimer's disease (AD), known as a chronic progressive neuronal degeneration disease, is the most common cause of dementia and usually affects people over the age of 60. AD progresses through different stages. The first stage, preclinical AD, is when the brain is still able to compensate for the damage to neurons caused by the disease so that no pathogenesis can be observed. When the brain is no longer able to compensate for the damage from AD, patients will progress into the stage of mild cognitive impairment (MCI). A common symptom of MCI is memory loss and difficulty with thinking, which gradually worsens over time. As the progression of AD goes on, patients will sequentially confront mild, moderate, and severe AD. In addition to aggravating memory loss, several psychological disorders, such as depression, agitation, and hallucination, will also appear, and patients will no longer be able to perform daily activities. Eventually, patients are prone to fatality due to the damage to basic physiological regulation [1]. The exact mechanism of AD is not fully understood.

Current research indicates that amyloid plaques and neurofibrillary tangles (NFTs) in the brain are the primary pathological phenomena of AD. These plaques and tangles ultimately break down the

Received 14 March 2024; accepted 24 June 2024.
Available online 13 September 2024

* Corresponding author. School of Pharmacy, China Medical University, Taichung 406040, Taiwan.
** Corresponding author. Department of Chemistry and Biochemistry, National Chung Cheng University, Chia-Yi 621301, Taiwan.
E-mail addresses: yihulin@mail.cmu.edu.tw (Y.-H. Lin), yelichen@ccu.edu.tw (Y.-L. Chen).
[1] Chun-Hsien Chen and Hsin-Hua Liang are equal contributions to this work.

https://doi.org/10.38212/2224-6614.3520

brain's structure, leading to cognitive decline and other symptoms associated with the disease. The cooperation of plaques and tangles increases the oxidative stress and induces the inflammatory reaction, which gradually causes irreversible synaptic dysfunction and neuronal death. Extracellular accumulation of advanced glycation end products (AGEs) by glycoxidation involving free radical production can be found in plaques. In addition, AGEs also facilitate the formation of plaques by cross-linking with amyloid beta (Aβ) aggregates [2]. The formation of plaques and NFTs can also trigger the secretion of proinflammatory cytokines by microglia and astrocytes. Subsequently, these cytokines induce inflammatory responses, which further cause dystrophic neuritis and eventually lead to neuronal degeneration [3]. The pathogeneses of plaques and NFTs start from the hippocampus, which is in charge of forming memory, and gradually spread throughout other parts of the brain [4].

According to the report from Alzheimer's Disease International, the number of people above 60 years old worldwide has reached nearly 900 million, and the population living with dementia is predicted to be approximately 152 million in 2050 [5,6]. The severity of AD has become not only a public health problem but also a social issue. Leqembi, the first Aβ-targeting antibody, was approved by the Food and Drug Administration to treat adult AD patients in 2023. However, Leqembi should be initiated in patients with MCI or mild dementia stage of AD [7]. Early and accurate diagnosis of AD is crucial for the development of effective AD therapies. Therefore, analyzing AD fluid biomarkers has become a popular research direction in recent years. These approaches can help detect the disease in its early stages and facilitate the development of targeted treatments.

2. Biomarkers of Alzheimer's disease

The National Association on Aging and Alzheimer's Disease proposed a research framework to biologically define AD by AT(N) biomarker profiles in 2018. The AT(N) scheme categorizes biomarkers into three groups based on the nature of the pathologic process. “A” refers to Aggregated Aβ evaluated by cerebrospinal fluid (CSF) $A\beta_{42}$, or $A\beta_{42}/A\beta_{40}$ ratio or amyloid positron emission tomography (PET). “T” refers to aggregated tau (NFTs) evaluated by CSF p-tau or Tau PET. “(N) refers to neurodegeneration or neuronal injury evaluated by anatomic magneticresonance imaging (MRI) or fluorodeoxyglucose (FDG) PET or CSF total tau [8]. The measured biomarkers for AD include the concentration of $A\beta_{42}$, $A\beta_{42}/A\beta_{40}$ ratio, total Tau protein (t-tau), and phosphorylated Tau protein (p-tau) 181 in CSF [9]. PET is valuable for evaluating the process of AD, but the need for radioactive substances limits its clinical use. Similarly, CSF sampling, which requires invasive lumbar punctures, is also impractical for routine use. Recently, a strategy focusing on blood-based biomarkers has gained attention from researchers [6].

Except for Aβ and Tau proteins as AD biomarkers, other biomarkers include DNA, RNA, and proteins originating from neuronal pathogenesis processes such as neuroinflammation, synaptic dysfunction, neuronal injury, and associated genetic variants could be helpful for early diagnosis of AD [10]. Given that many of these biomarkers also indicate other neurodegenerative diseases, numerous studies have explored their correlations with core AD biomarkers to enhance clinical interpretations [11–13]. Hawksworth et al. conducted a recent review focusing on protein biomarkers of AD, emphasizing their associations with amyloid or tau pathology, as well as cognitive deficits in AD [14]. In this context, we introduce Aβ, Tau proteins, and several potential AD biomarkers.

2.1. Amyloid-beta

Aβ peptides are short peptide chains produced when amyloid precursor protein (APP) is broken down through proteolysis. APP is a membrane protein that is commonly found in synapses. Although the exact function of APP is not yet fully understood, it is believed to play a role in supporting the growth of neurons and synapses, as well as acting as a receptor within cells [15,16]. The metabolism of APP is regulated by three types of secretase enzymes - α-secretase, β-secretase, and γ-secretase. Approximately 90% of APPs are metabolized by α-secretase and γ-secretase, which produces soluble peptide residues that are easier to eliminate from the body. It has been observed that around 10% of APPs are metabolized by β-secretase and γ-secretase [17]. When β-secretase hydrolyzes APPs, it generates longer and hydrophobic peptide residues (Aβ) that tend to clump together and are difficult to eliminate from the body. This process is also known as amyloidogenesis. The Aβ family can have different lengths due to the imprecise cleaving site of APP by γ-secretase. These lengths can range from 36 to 43 amino acids. $A\beta_{40}$ accounts for approximately 80–90% of Aβs produced, while $A\beta_{42}$ accounts for approximately 5–10% [17,18]. When Aβs fail to be effectively eliminated, they self-aggregate from monomers to plaques via oligomers and fibrils [19].

In AD patients, unknown or genetic mutations cause increased β-secretase activity, resulting in excessive accumulation of Aβ. On the other hand, the oligomeric forms of Aβ (AβO) can lead to various neuronal damages, such as receptor-mediated toxicity, dysregulation of ion channels, proteasome impairment, and mitochondrial dysfunction. These damages eventually induce the pathogenesis of AD [20].

In current clinical scenarios, PET can be used to visualize the distribution of Aβ and the atrophying structure of the brain [1], and the levels of $A\beta_{42}$ or the ratio of $A\beta_{42}$ to $A\beta_{40}$ in CSF or plasma is measured by suitable analytical methods for AD diagnosis [21−24]. These values can help evaluate the progression of AD in the clinical setting and were integrated in Table 1. AβO plays a crucial role in AD development and is considered a potential diagnostic candidate. The AβO in plasma measured using a multimer detection system-oligomeric assay was compared between 52 AD patients treated and 52 individuals with normal cognition. The cut-off value for AβO is $\geq$ 0.78 ng/mL [25]. A significant 3- to 5-fold increase in AβO has been detected in CSF of AD patients (63) compared to controls (54). The AβO in CSF ranged between 0.1 and 10 pg/mL [26].

2.2. Tau protein

Tau protein is generated in the brain through the transcription of the microtubule-associated protein tau (MAPT) gene on human chromosome 17. There are six isoforms of water-soluble, non-folded proteins, including Tau352 (0N3R), Tau381 (1N3R), Tau410 (2N3R), Tau383 (0N4R), Tau412 (1N4R) and Tau441 (2N4R) [27]. The function of Tau protein was used to support the structure of microtubes, which dominate the transportation of nutrients throughout neurons in the brain. As Tau proteins are phosphorylated, they collapse from microtubes and twist into tangles to form the NFTs. Subsequently, the structure of microtubes will disintegrate and disrupt the transportation of nutrients. Eventually, the gradual neuronal death in the brain will occur due to the dysfunction of microtubes and the neurotoxicity of tangles [18]. Phosphorylation is the most common post-translational modification of Tau protein. Other modifications include glycosylation, nitration, and proteolysis. Tau441 contains 85 potential phosphorylation sites, with 45 serine (S), 35 threonine (T), and 5 tyrosine (Y) sites. These sites are concentrated in the proline-rich region and microtubule-binding repeat region [28,29]. When

Table 1. Clinical research of biomarkers of AD in CSF and plasma samples.

Biomarker	Sample	Detection outcome		Cut-off value	Reference
		NC [a]	AD [b]		
$A\beta_{42}$	CSF	916 ± 182 pg/mL (*ApoE* ε4-) 745 ± 205 pg/mL (*ApoE* ε4+)	507 ± 180 pg/mL (*ApoE* ε4-) 460 ± 137 pg/mL (*ApoE* ε4+)	≤ 550 pg/mL	[22]
t-tau		276 ± 116 pg/mL (*ApoE* ε4-) 300 ± 161 pg/mL (*ApoE* ε4+)	804 ± 404 pg/mL (*ApoE* ε4-) 792 ± 484 pg/mL (*ApoE* ε4+)	≥ 375 pg/mL	
p-tau		44 ± 14 pg/mL (*ApoE* ε4-) 50 ± 23 pg/mL (*ApoE* ε4+)	91 ± 39 pg/mL (*ApoE* ε4-) 89 ± 39 pg/mL (*ApoE* ε4+)	≥ 52 pg/mL	
$A\beta_{40}$	CSF	6.7 ± 2.5 ng/mL	5.9 ± 2.3 ng/mL	-	[23]
$A\beta_{42}$		0.87 ± 0.36 ng/mL	0.67 ± 0.26 ng/mL	≤ 0.64 ng/mL	
$A\beta_{42}/A\beta_{40}$		1.5 ± 1.1	1.3 ± 0.66	≤ 0.95	
$A\beta_{40}$	CSF	1935 pg/mL (cohort 1) 1996 pg/mL (cohort 2)	2088 pg/mL (cohort 1) 2249 pg/mL (cohort 2)	-	[26]
$A\beta_{42}$		44 pg/mL (cohort 1) 114 pg/mL (cohort 2)	108 pg/mL (cohort 1) 216 pg/mL (cohort 2)		
AβO (ADDLs)		0.28 (0.18-0.34) pg/mL (cohort 1) 0.52 (0.41-0.66) pg/mL (cohort 2)	2.6 (0.75-3.3) pg/mL (cohort 1) 1.52 (1.19-1.94) pg/mL (cohort 2)		
$A\beta_{42}$	CSF	503.99 ± 156.67 pg/mL	328.76 ± 110.54 pg/mL	≤ 416.0 pg/mL	[35]
t-tau		86.03 ± 47.47 pg/mL	145.69 ± 80.22 pg/mL	≥ 76.7 pg/mL	
p-tau		41.59 ± 21.81 pg/mL	66.72 ± 35.82 pg/mL	≥ 36.1 pg/mL	
$A\beta_{42}$/p-tau		14.38 ± 6.46	7.39 ± 7.39	≤ 9.53	
$A\beta_{42}$/t-tau		7.12 ± 3.48	3.45 ± 4.01	≤ 4.13	
$A\beta_{40}$	Plasma	60.3 ± 7.2 pg/mL	43.9 ± 22.6 pg/mL	-	[24]
$A\beta_{42}$		15.8 ± 0.7 pg/mL	23.5 ± 18.8 pg/mL	≥ 16.41 pg/mL	
Tau		13.3 ± 6.9 pg/mL	47.6 ± 19.2 pg/mL	≥ 24.90 pg/mL	
$A\beta_{42}/A\beta_{40}$		0.267 ± 0.038	0.557 ± 0.231	≥ 0.361	
AβO	Plasma	0.45 ± 0.19 ng/mL	1.43 ± 0.30 ng/mL	≥ 0.78 ng/mL	[25]

Abbreviations: ADDLs: amyloid-derived diffusible ligands.
[a] Normal control
[b] Patient with a dementia due to AD.

the Tau protein appears hyperphosphorylated, it reduces its affinity with microtubules. Consequently, the Tau protein gets released into the cell [30]. This leads to an increase in the concentration of both t-tau and p-tau compared to normal individuals. P-tau inCSF, mainly p-tau181, p-tau217, and p-tau231, is considered an important biomarker for AD and has been included in the diagnostic criteria [31]. Several studies have reported that p-tau217 and p-tau231 in CSF may be better diagnostic biomarkers for AD than p-tau181 [32,33]. In addition, p-tau217 in plasma performs better as an AD diagnostic biomarker than p-tau181 and p-tau231 [34]. Clinically relevant concentrations of Tau protein in CSF and plasma were integrated in Table 1.

2.3. Neurofilament light chain

Neurofilament light chain (NfL) is one of the four subunits of axonal cytoskeletal protein, released upon axonal damage and detectable in both CSF and plasma [36]. Given that various neurological diseases and aging entail this pathological process, NfL levels cannot reliably differentiate AD from other conditions but can aid in early diagnosis [37]. Jung et al. noted that the longitudinal changes in NfL levels can reflect and predict the severity of AD, categorizing NfL as a monitoring biomarker for AD per the definitions of the FDA-NIH Biomarker Working Group in 2016 [38]. Notably, the measurability of NfL in blood underscores its significance for in-depth discussion [39]. Multiple studies have confirmed plasma NfL as a potential AD biomarker, with its dynamics predictive not only of cortical atrophy and neurogenesis in the presymptomatic stage but also of white/grey matter atrophy in symptomatic AD patients [37,40–42]. Moreover, while NfL exists in multiple forms, its complete characterization remains ongoing. Budelier et al. observed significant differences in concentrations of neurofilament light fragments between AD patients and healthy individuals CSF, including NfL165, NfL324, and NfL530 by immunoprecipitation-mass spectrometry assay and the commercially available immunoassay [43].

2.4. Neurogranin

Neurogranin (Ng) is a postsynaptic protein that binds to calmodulin, initiating signaling pathways crucial for synaptic plasticity, synaptic regeneration, and long-term potentiation [44]. Ng is predominantly found in the hippocampus and cerebral cortex, and elevated CSF levels indicate synaptic loss, leading to cognitive decline. A recent post-mortem study of human brain tissue revealed reduced Ng levels in cognitive brain regions in AD and healthy aging cohorts, supporting the notion that CSF Ng reflects synaptic loss in the brain and serves as a hallmark of cognitive decline [45]. Tarawneh et al. compared symptomatic AD patients with cognitively normal groups and concluded that CSF Ng is associated with other CSF markers, representing a promising marker for synaptic dysfunction in AD [46]. Wellington et al. observed Ng level differences in typical and atypical AD patients; Ng levels were higher in amnestic AD and lower in AD with posterior cortical atrophy. They also identified distinct relationships between Ng, t-tau, and NfL, suggesting that Ng levels may aid in characterizing various AD phenotypes [47]. However, it is worth noting that the specificity of CSF Ng for AD is controversial, as CSF Ng levels are also elevated in aging and MCI cohorts [48]. Nonetheless, Ng still holds promise as a prognostic biomarker for early AD diagnosis, although further research and evidence are required.

2.5. α-Synuclein and β-synuclein

The synuclein family comprises α-synuclein (αSyn), β-synuclein (βSyn), and γ-synuclein (γSyn), among which αSyn binds to synaptic vesicles, facilitating soluble N-ethylmaleimide-sensitive factor attachment protein receptor (SNARE) complex assembly to regulate neurotransmitter release [49]. Typically, the α-helical form of αSyn exhibits membrane binding, while the unstructured form remains soluble in the cytosol [50]. The transformation between these two forms is modulated by βSyn and γSyn. Pathologically, αSyn aggregates into oligomers or fibrils, leading to neurotoxicity and contributing to synucleinopathy, a hallmark of Parkinson's disease [49,51]. In AD, CSF levels of αSyn are strongly correlated with the triple core CSF markers (t-tau, p-tau181, and Aβ), with CSF αSyn levels increasing as MCI progresses to symptomatic AD, thus supporting the utility of CSF αSyn for early or differential diagnosis [52,53]. Majbour et al. observed increased total αSyn CSF levels in AD, with no changes in oligomeric or fibrillar forms, suggesting variations arise from the soluble form of αSyn; notably, AD patients did not exhibit synucleinopathy as seen in Parkinson's disease [54]. Elevated levels of βSyn and γSyn have also been detected in the CSF of AD patients, with βSyn showing correlations with Tau proteins; furthermore, βSyn is detectable in blood, indicating its potential as an alternative AD marker [55].

2.6. Soluble triggering receptor expressed on myeloid cell 2

Neuroinflammation marker proteins are promising biomarkers for early AD diagnosis, including soluble triggering receptor expressed on myeloid cells 2 (sTREM2), glial fibrillary acidic protein (GFAP), YKL-40, and others. Neuroinflammation, characterized by dysregulation of the central nervous system immunity, primarily involves microglial cells and astrocytes [56,57].

In AD, the aggregation of Aβ and deposition of other proteins in brain tissues are neurotoxic, triggering microglial cells to engage in phagocytosis and activating astrocytes to sustain overall neuronal function [56]. Pathologically, the imbalance between pro-inflammatory and anti-inflammatory responses results in the transcriptional activation of downstream genes and the overproduction of toxic factors, ultimately leading to neuronal death [57]. TREM2, expressed on the surface of microglia, plays a crucial role in recognition. Its soluble cleavage product, sTREM2, detectable in CSF, serves as a marker of microglial activation in AD. Knapskog et al. found that elevated CSF levels of sTREM2 are associated with aging and tauopathy but not cognitive status [58]. Various studies have reported decreased sTREM2 levels in the CSF of AD patients, with individual baseline levels varying [59–61]. Nevertheless, sTREM2 remains a potential biomarker for investigating the dual role of microglia in AD pathology [62].

Moreover, TREM2 is among the gene variant expression targets of microglia and has been reported to be regulated by multiple AD risk genes in different studies. TREM2 levels are higher in carriers of the rs7748513 or R47H variants, lower in L2112P carriers, and unaffected in apolipoprotein E gene ε4 (*ApoE4*) carriers [61,63,64]. Kim et al. studied an autopsy-confirmed cohort and found that TREM2 variants were associated with atypical AD clinical phenotypes and accelerated global cognitive decline [65]. Deming et al. discovered an association between variants in the membrane-spanning 4-domains subfamily A (MS4A) gene region and CSF sTREM2 levels, including the single nucleotide polymorphism rs1582763 [66].

2.7. GFAP and YKL-40

GFAP is an intermediate filament protein present in the cytoskeleton of astrocytes, overexpressed in reactive astrocytes and astrogliosis. Its levels in CSF or plasma can reflect astrocyte status, with reduced GFAP indicating decreased astrocyte activity [57]. In AD and other neurodegenerative conditions, GFAP levels are elevated in both plasma and CSF. Given the convenience of blood-based biomarkers for clinical monitoring and research, most studies have focused on the reliability of plasma GFAP for AD diagnosis [67,68]. Yang et al. found that plasma GFAP exhibited stronger potential for screening AD amyloid pathology compared to other plasma biomarkers, such as p-tau181 and NfL, and showed prognostic power in predicting future cognitive decline [69]. Chatterjee et al. reported alterations in GFAP and other plasma markers both cross-sectionally and longitudinally in AD, collectively providing improved predictive capability for Aβ pathological status [70]. Stevenson-Hoare et al. obtained similar results and also noted a close association between plasma GFAP levels and AD risk genes such as *ApoE4* [71]. Taken together, these studies suggest that plasma GFAP could serve as a diagnostic and predictive biomarker for AD.

Another astrocyte biomarker under discussion is YKL-40, also known as chitinase-3-like protein 1 (CHI3L1), which can be detected in CSF and plasma [67]. YKL-40 is a secreted glycoprotein of 40 kDa involved in various inflammatory pathways associated with conditions such as rheumatoid arthritis, cancers, and neurological diseases [72]. Pelkmans et al. identified a greater role for YKL-40 in mediating Aβ-induced tau phosphorylation and neuronal injury, while GFAP mediates early Aβ misfolding [68]. In a clinical trial investigating inflammatory plasma markers, preclinical AD patients showed significantly higher plasma levels of both GFAP and YKL-40, indicating that these markers could help identify individuals at risk of developing AD [57,73]. Although YKL-40 is gaining recognition as a potential early diagnostic biomarker for AD, further research is needed to fully understand its role, significance, and correlation with other biomarkers.

2.8. Transactive response DNA binding protein of 43 kDa

Transactive response DNA binding protein of 43 kDa (TDP-43), an intranuclear protein encoded by the TAR DNA Binding Protein (TARDBP) gene, is associated with TDP-43-mediated RNA splicing, trafficking, stabilization, and regulation of gene expression [74]. Mutations in TDP-43-related genes are linked to amyotrophic lateral sclerosis and frontotemporal lobar degeneration, leading to symptoms such as muscle weakness and personality changes [11]. Additionally, TDP-43 pathology has been observed to form deposits in the brains of individuals aged 80 years and older, termed limbic

predominant age-related TDP-43 encephalopathy (LATE) [74]. LATE coexisting with AD, known as LATE + AD, is common in AD patients with accelerated cognitive decline, and TDP-43 may also trigger neuroinflammation in the brain [75]. Noteworthy, TDP-43 pathology is also common in other subtypes of AD and is involved in AD progression. TDP-43 directly interacts with Aβ and Tau proteins, cross-seeding and co-localizing with them to form oligomers and aggregates [74]. Genetically, TDP-43 pathology is associated with the *ApoE4*, and the burden of TDP-43 increases with the number of *ApoE4* alleles, collectively accelerating the development of AD-type pathology. Altogether, TDP-43 serves as a significant risk factor of AD and plays a role in the progression for AD-type dementia [74].

2.9. Genetic risk factors

In addition to the extensively studied genetic risk factors such as *ApoE* and the previously mentioned gene variants, as well as the early-discovered APP, PSEN1, and PSEN2 mutations [76,77], other gene variants, including *SORL1*, *ABCA7*, *ABCA1*, *PLCγ2*, and *ADAM10*, are also associated with AD risk. Many of these variants are rare and are linked to factors such as age, sex, or race [78]. The discovery of numerous genes affecting AD provides multiple avenues for a comprehensive and diverse understanding of the disease [76].

A recent meta-analysis, combining data from previous genome-wide association studies with findings from a new large case–control study, identified 42 new risk loci and confirmed 33 known loci for AD [76]. Furthermore, this analysis highlighted the involvement of these loci in pathways related to amyloid, tau, and microglia, further elucidating the molecular mechanisms underlying AD pathogenesis [76].

2.9.1. ApoE

Corder et al. indicated that individuals who possess the genetic variant ε4 in the *ApoE* gene have a higher frequency in AD patients with late-onset Alzheimer's disease (LOAD) [79]. The *ApoE* gene, located on chromosome 19, has three alleles: ε2, ε3, and ε4. These alleles are generated by two single-nucleotide polymorphisms (SNPs), rs429358 (C/T) and rs7412 (C/T). The *ApoE* genotype ε3 is the most common in the general population, accounting for 50–90%, followed by ε4 at 5–35% and ε2 at 1–5%. An antagonistic effect that reduces the risk of AD can be observed in carriers of *ApoE*-ε2, while carriers of *ApoE*-ε3 do not show any influence on AD. However, carriers of *ApoE*-ε4 have a higher risk of suffering from AD. Individuals who are heterozygous for ε4 have a 2–3 times higher risk of developing AD, and this risk increases to 8–12 times for those who are homozygous for ε4 [80].

2.9.2. MicroRNAs

MicroRNAs (miRNAs) are non-coding RNA molecules approximately 22–23 nucleotides in length that play crucial roles in regulating gene expression. miRNAs detected in CSF, blood, and brain tissues have shown stability and are being investigated as candidate biomarkers for AD, although their precise relationships with AD pathology are not yet fully understood [81–83]. Swarbrick et al. identified miRNAs as predominantly involved in AD pathological pathways, including those related to amyloid, tau, and neuroinflammatory signaling pathways. They also reported dysregulated miRNA expression in the peripheral blood of AD patients [84]. In a systematic review, Van den Berg et al. identified 253 circulating miRNAs with various functions, such as upregulation, downregulation, or dual-functionality. They noted differences in expression levels between AD patients and healthy controls [83]. For example, the miR-29 family is believed to downregulate β-site amyloid precursor protein-cleaving enzyme 1 (BACE1) [85]. Additionally, miR-125b-5p has been implicated in inducing tau phosphorylation, potentially contributing to glial proliferation and synapse-related dysfunction [86–88]. Furthermore, miR-146a-5p levels were found to be elevated in both the brains and blood of AD patients, promoting neuroinflammation and neurodegeneration [81,86].

3. Nanomaterial-based optical sensors

The low trace levels of biomarkers in body fluids make it challenging to detect them accurately. Fortunately, optical sensors have emerged as highly sensitive tools that can swiftly detect the slightest changes in biomarker levels. They are an excellent alternative to conventional instruments due to their adaptability and ability to provide reliable results. Nanomaterials are often employed in sensors to amplify the signal and enhance sensitivity. With these benefits, nanomaterials-based optical sensors, including colorimetric, fluorescent, and surface-enhanced Raman scattering (SERS) sensors, have been developed to detect AD biomarkers.

3.1. Colorimetric sensors

Colorimetric sensors transform biochemical reactions occurring during the sensing process into observable color changes, which can be quantified

through alterations in absorption spectra or visually observed without the need for specialized equipment [89,90]. Typically, the biochemical events induced by target analytes cause changes in the electronic energy of chromogens or alter the surrounding dielectric environment of metal nanoparticles, resulting in changes in absorbance or shifts in the absorption peak. The absorbance change is directly proportional to the concentration of the target analyte, making colorimetric sensors ideal for quantitative, label-free, real-time monitoring, and easy implementation [89,91,92]. Therefore, the selection of chromogenic substrates with distinct color transitions is crucial for their efficacy. Upon reviewing previously published colorimetric sensors for AD biomarkers, the primary substrates utilized include chromogenic indicators coupled with peroxidase-activity enzymes and plasmonic particles, such as noble metal nanoparticles (shown in Fig. 1).

3.1.1. Oxidative enzyme based colorimetric sensor

In the context of colorimetric sensors employing chromogens, color transitions may occur through enzymatic catalysis, pH mediation, or other mechanisms [89]. For instance, Khachornsakkul et al. utilized bromocresol purple (BCP) as a sensing element and employed a dry-protein binding process for the detection of urine Aβ [93]. BCP, with a pKa of 6.3, exhibits a yellow color below pH 5.2 and violet above pH 6.8 [94]. In the pH 5 sensing system, BCP and Aβ interact via electrostatic forces, causing BCP to increase its conjugation degree and reduce the π^* state energy, resulting in a color change from yellow to blue-purple. Consequently, there is a bathochromic and hyperchromic shift in its absorption spectrum. The proposed sensing system also incorporates BCP onto a distance-based paper analytical device (dPAD). The dPAD uses a self-designed pattern, wax-printed on filter paper, and consists of two functional areas: a sample inlet and a longitudinal detection area coated with BCP. When Aβ flows through the detection channel through capillary action, it binds to BCP, causing a color change. The higher the concentration of target Aβ, the longer the length of the color-changing zone, which facilitates quantitative analysis [93].

Certain chromogenic substrates undergo color transitions catalyzed by oxidative enzymes. One such substrate is 3,3′,5,5′-tetramethylbenzidine (TMB), a well-known peroxidase substrate widely used in colorimetric and enzymatic assays [95]. TMB exhibits various colors depending on its oxidation state, appearing transparent (with absorbance at 285 nm) as diamine (TMB), blue-green (at 370 nm and 652 nm) as a charge−transfer complex (TMB^{1+}), and yellow (at 450 nm) as diimine (TMB^{2+}) [96]. This chromatic variability of TMB has also been harnessed in colorimetric sensors for AD diagnosis.

The colorimetric signals of the tau protein aptasensor introduced by Duan et al. were generated through the oxidation of TMB catalyzed by horseradish peroxidase (HRP). To enhance the signal, they designed a double-stranded nanostructure known as polyvalent biotinylated aptamer scaffold (PBAS), as shown in Fig. 2. PBAS consists of numerous biotinylated Tau protein aptamers hybridized with linker DNAs, where the biotin labels can be attached to streptavidin-modified magnetic beads for separation or streptavidin-modified HRP

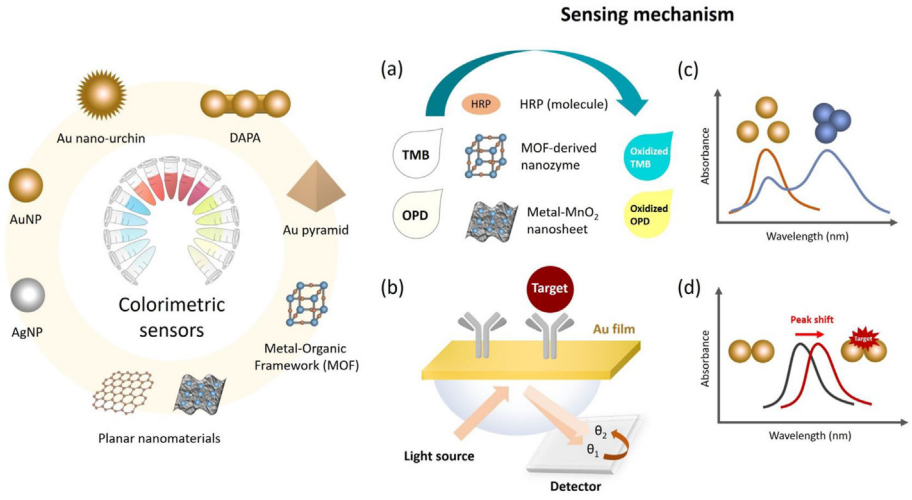

Fig. 1. Colorimetric strategies for AD biomarkers based on nanomaterials with different mechanisms. (a) Oxidative enzyme based colorimetric sensor. (b) Surface plasmon resonance. (c) Self-aggregation of nanomaterials based colorimetric sensor. (d) Localized surface plasmon resonance.

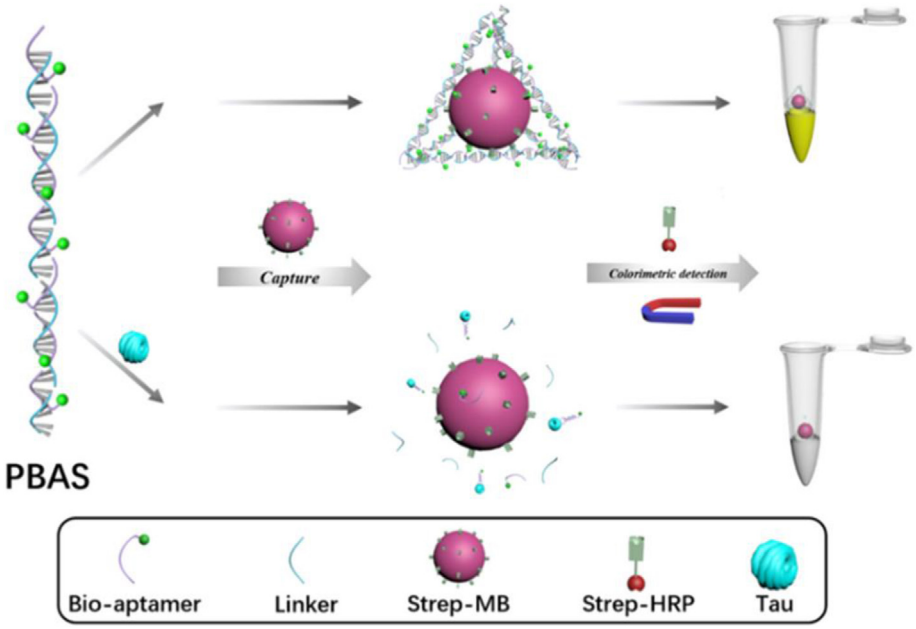

Fig. 2. Schematic illustration of the PBAS-based colorimetric assay of Tau proteins. Reprinted with permission from Polyvalent Biotinylated Aptamer Scaffold for Rapid and Sensitive Detection of Tau Proteins (Ref [97]). Copyright 2020 American Chemical Society.

(strep-HRP) for catalysis. This configuration provides multiple effects on surface immobilization, target recognition, and signal amplification. In the absence of Tau proteins, PBAS forms enzymatic clusters that catalyze TMB oxidation, resulting in a color transition from colorless to yellow (450 nm). However, when target Tau proteins bind to the aptamer, they prevent the formation of PBAS, leading to a reduction in strep-HRP levels and decreased catalytic activity on TMB. Furthermore, the authors compared PBAS with monovalent biotinylated aptamers (MBA) and methods using hybridization chain reaction (HCR). The PBAS-based aptasensor showed rapid and efficient signal amplification, producing signals four times greater than the MBA-based method, demonstrating its superior efficiency [97]. Chen et al. also combined signal amplification with TMB in the proposed aptasensor for the detection of AβO in CSF. They adopted a cyclic amplification approach involving an AβO-specific aptamer, four single-stranded DNA (ssDNA) probes, Exonuclease III (Exo III), and nicking endonucleases (Nt.Alw1). Initially, AβO-specific aptamer forms triple-helix with single-strand DNA. In the presence of AβO, the triplex-helix disintegrates, aptamer captures AβO, single-strand DNA is released, which then initiates a dual-cyclic amplification cascade. This process involves a series of hybridization and cleavage steps, using enzymes like Exo III and Nt.Alw1 to cleave fragments, which are then reused for repeated hybridization cycles. After two cycles of amplification, the final products contain numerous G-quadruplexes. These G-quadruplexes form complexes with heme, acting as DNAzymes with peroxidase properties that catalyze TMB oxidation in the presence of H_2O_2. The absorbance of blue oxidized TMB at 650 nm can be measured to determine AβO levels in CSF with high sensitivity and specificity [98].

Another colorimetric sensor based on HRP-TMB, developed by Khan et al., offers a method for detecting $A\beta_{40}$ without the need for antibodies or other recognition elements. They utilize the specific binding affinity of $A\beta_{40}$ to gold nanoparticles (AuNPs) and various metal ions. In this assay, citrate-capped AuNPs capture $A\beta_{40}$, forming complexes. Metal ions are then added, not to induce AuNP aggregation but to attach to $A\beta_{40}$ through electrostatic attraction, enabling an indirect colorimetric signal output. Nickel (Ni) is used as the source of metal ions, conjugated with HRP (Ni-HRP), which catalyzes the oxidation of TMB, producing a colorimetric signal. Thus, $A\beta_{40}$ binds to both AuNPs and Ni-HRP, forming a sandwich-like complex that allows the quantification of $A\beta_{40}$ in human serum. Additionally, to select the optimal metal ion, the minimum aggregatory concentration of AuNPs with different metal ions was investigated, including Nickel (Ni), Copper (Cu), Zinc (Zn), and Cadmium (Cd). Ni was chosen because it provides optimal binding to $A\beta_{40}$ without causing AuNP

aggregation, ensuring that the color changes in the sensing system originate from TMB oxidation [99].

In addition to natural enzymes, nanozymes have emerged as promising tools for biosensor development based on enzyme–substrate reactions. Nanozymes are nanomaterials that mimic enzyme-like functions, including hydrolases, oxidoreductases, and transferases. They offer advantages in synthesis, design, modification, stability, and adjustable catalysis [95,100]. Among nanozymes, metal-based nanomaterials with peroxidase activities have been extensively explored [101].

Zhou et al. synthesized porous crystalline materials known as ZnO–Co_3O_4 nanocages (NCs) and employed them as nanozymes for a colorimetric sensor targeting Aβ [102]. These ZnO–Co_3O_4 NCs, derived from metal–organic frameworks (MOFs) through oxidation, possess unique stability characteristics compared to traditional MOFs [103], as they can prevent disassembly due to potential ligand exchange during the sensing process. The metal nodes of $ZnCo_3O_4$ NCs exhibit peroxidase activity and can catalyze TMB, leading to a color change from colorless to blue-green (652 nm). Additionally, both Zn^{2+} and Co^{3+} exhibit binding affinity toward Aβ monomers. Consequently, the activity of the nanozyme is inhibited by the binding of Aβ monomers, resulting in a decrease in the absorbance intensity of TMB at 652 nm. Furthermore, Aβ species such as oligomers and fibrils exhibit lower binding affinity to nanozymes. Therefore, monitoring changes in TMB absorbance intensity enables quantitative analysis of Aβ and monitoring of amyloidogenesis [102].

Hu et al. discovered that different Aβ species modulate the peroxidative activity of MnO_2 nanosheets to varying degrees. Building on this finding, they developed an enzymatic colorimetric sensor array for versatile detection of Aβ species ($Aβ_{40}$, $Aβ_{42}$, Pro-$Aβ_{42}$, $Aβ_{42}$ fibrils, AβE22G, and Pro-AβArc). In this sensing array, colorimetric signals arise from the oxidation of o-phenylenediamine, catalyzed by MnO_2 nanosheets, resulting in a color change from colorless to yellow (absorbance at 450 nm). Additionally, since different Aβ species exhibit distinct binding forces with MnO_2 nanosheets, MnO_2 nanosheets are conjugated with various types of metal ions (Zn^{2+}, Fe^{3+}, or Cu^{2+}) to expand the differences in binding affinities of the six Aβ species for linear discriminant analysis. As a result, the sensor array can distinguish and quantify the six types of Aβ species, allowing for monitoring of the Aβ aggregation process [104].

According to the review presented above (Table 2), oxidative enzyme based colorimetric biosensors for detecting AD biomarkers are diverse, mainly utilizing chromogenic substrates, peroxidase enzymes, metallic and composite nanomaterials, and various sensing strategies such as homogeneous assays, paper-based devices, signal amplification, and optical arrays. While not all methods incorporate recognition elements, these approaches have demonstrated specificity for target markers and have been applied in both simulated and real biological samples. They offer sensing advantages including label-free detection, visual observation, and sensitivity.

3.1.2. *Localized surface plasmon resonance*

Localized surface plasmon resonance (LSPR) refers to the collective oscillation of free electrons on the surface of nanoparticles, typically metal nanoparticles such as gold (Au) or silver (Ag), when illuminated with light of a specific wavelength. This phenomenon leads to enhanced absorption and scattering of light at certain wavelengths, known as the plasmon resonance wavelength, which is highly sensitive to the size, shape, and composition of the nanoparticles [91,105]. Consequently, the optical properties of AuNPs induced by LSPR find wide applications in the development of biosensors for

Table 2. Nanomaterial-based colorimetric (absorbance) sensors for AD biomarkers.

Nanomaterials	Biomarkers	Recognition element	Limit of detection	Sample	References
AuNPs	$Aβ_{40}$	–	0.23 nM	Human serum	[99]
ZnO–Co_3O_4 nanocages	$Aβ_{40}$	–	3.5 nM	Rat CSF	[102]
Metal ion conjugated MnO_2 nanosheet	Aβ species	–	0.44 pM	Human blood	[104]
AuNPs	AβO	Aptamer	0.56 nM	aCSF	[107]
pA-pT-apt@AuNPs	AβO	Aptamer	3.03 nM	aCSF	[108]
AgNPs, AuNPs	$Aβ_{40}$, $Aβ_{42}$	–	–	Human plasma	[109]
Gelsolin modified AgNTs and AgNRs	$Aβ_{40}$, $Aβ_{42}$	–	–	Rat CSF and brain tissue	[111]

Abbreviations: aCSF: artificial cerebrospinal fluid, AgNPs: silver nanoparticles, AgNRs: silver nanorods, AgNTs: silver nanotriangles, AuNPs: gold nanoparticles, pA-pT-apt@AuNPs: aptamer-polythymine- polyadenine-gold nanoparticles, PBAS: polyvalent biotinylated aptamer scaffold.

AD biomarkers [90,92]. AuNPs-based colorimetric sensors leverage the absorbance of plasmonic AuNPs and monitor absorption changes for analysis. One commonly utilized strategy is aggregation-mediated color-tuning. The absorption band of dispersed AuNPs typically occurs at 520 nm, appearing as a red color, while aggregation leads to a color shift towards purple or blue hues [106].

Zhu et al. employed citrate-capped AuNPs to develop a label-free colorimetric aptasensor for detecting AβO. Upon the addition of Na^+ and aptamer, the negatively charged surface of AuNPs is neutralized, leading to aggregation and causing a shift in absorption spectra from 520 nm (red) to 650 nm (purple). In the presence of AβO, the aptamer forms complexes with AβO, stabilizing AuNPs against salt-induced aggregation. As the amount of AβO increases, the ratio of absorbance at 650 nm−520 nm (A_{650}/A_{520}) decreases, resulting in a series of color changes (from purple to ruby red). Therefore, the A_{650}/A_{520} ratio reflects the degree of aggregation and can be used to quantify the amount of AβO [21,107]. Another AβO aptasensor, devised by Tu et al., utilized elongated aptamers, AuNPs, and a salt-induced aggregation strategy. The aptamer is extended with polythymine (pT) and polyadenine (pA), where the terminal pA preferentially anchors the aptamer on AuNPs to prevent the aptamer from interacting directly or randomly with the AuNPs surface; pT serves as a spacer to provide space between adjacent aptamers (pA-pT-apt@AuNPs). With the assistance of the pA-pT sequence, the aptamer on the other end is allowed to form an upright conformation on AuNPs, meaning the aptamer is stretched and stands up from the surface of the AuNPs, resulting in a significant increase in the size of AuNPs. This design preserves space for target recognition and improves sensing specificity and efficiency. In the presence of AβO, the aptamer undergoes adaptive folding, stabilizing and preventing pA-pT-apt@AuNPs from $MgCl_2$-induced aggregation. Consequently, the initially aggregated AuNPs transition into a dispersed state, changing the color from blue to red [108].

Ghasemi et al. took a different approach by utilizing two types of plasmonic nanoparticles, silver nanoparticles (AgNPs) and AuNPs, to detect and differentiate between $Aβ_{40}$ and $Aβ_{42}$, as well as human serum albumin in plasma [109]. $Aβ_{40}$ and $Aβ_{42}$ have an isoelectric point of 5.3 [110], rendering them positively charged and showing varying binding affinities towards citrate-capped nanoparticles, thereby aiding in the dispersion of nanoparticles. Copper ions are introduced to induce nanoparticle aggregation by bridging with $Aβ_{40}$ and $Aβ_{42}$, resulting in distinct spectral and color changes for the two plasmonic nanoparticles. The original and emerging absorption peaks are at 520 nm and 620 nm for AuNPs, and at 390 nm and 500 nm for AgNPs. By combining these colorimetric responses of the two metal nanoparticles and recording the absorbance at three wavelengths (420 nm, 530 nm, 620 nm), the color patterns and data matrix of $Aβ_{40}$ and $Aβ_{42}$ are established for linear discriminant analysis of $Aβ_{40}/Aβ_{42}$ quantification [109]. Similarly, Liu et al. presented a colorimetric sensor for CSF $Aβ_{40}$ and $Aβ_{42}$ without the use of recognition elements [111]. They designed rod- and triangle-shaped AgNPs, named AgNRs and AgNTs, respectively, and modified their surfaces with gelsolin, which has affinity for $Aβ_{40}$ and $Aβ_{42}$. The gelsolin-modified AgNPs serve as the sensing elements, with characteristic SPR peaks at 514 nm (AgNRs) and 640 nm (AgNTs). In the presence of $Aβ_{40}$ or $Aβ_{42}$, the gelsolin-modified AgNRs or AgNTs aggregate upon binding with the target peptides, causing shifts in the absorption bands and various color transitions. Specifically, AgNRs exhibit new absorption bands around 700 nm and change color from red to purple (with $Aβ_{40}$) or blue (with $Aβ_{42}$). AgNTs show new absorption bands around 900 nm and change color from dark blue to light blue (with $Aβ_{40}$) or light gray (with $Aβ_{42}$). By evaluating these color changes in parallel, the sensor produces specific color response patterns that can simultaneously identify and distinguish $Aβ_{40}$ and $Aβ_{42}$ [111].

As mentioned, LSPR is closely tied to the structure, composition, particle−particle distance, and dielectric environment of metallic nanoparticles, all of which influence the effect and optical signatures of LSPR. Various nanostructures of AuNPs have been utilized to modulate color for biosensing applications [91,105]. Nair et al. introduced Au nano-urchins, Au nanomaterials with a spiky structure, for detecting the fibrillation process of $Aβ_{42}$ starting from trace amounts of $Aβ_{42}$ monomers. The urchin-like nanostructure offers a larger surface area and enhanced field enhancement at the tips, enabling them to detect very low concentrations of $Aβ_{42}$. By simply mixing the Au nano-urchin solution with the $Aβ_{42}$ monomer solution in a cuvette, the fibrillation process is monitored over time using an optical fiber and lens assembly. When fibrils begin to form and attach to the Au nano-urchins, the plasmonic response of the Au nano-urchins is impeded, leading to a more pronounced reduction in LSPR peak intensity (650 nm) compared to spherical AuNPs. These absorbance changes can be observed in as little as 5 min, indicating the potential for sensing

Aβ fibrils [112]. Kim et al. developed a multiplex LSPR sensor employing antibodies and three different shapes of AuNPs for the simultaneous detection of $A\beta_{40}$, $A\beta_{42}$, and tau protein. AuNPs are synthesized in spherical shapes (54 nm), short rods (aspect ratio 1.6), or long rods (aspect ratio 3.6), and then PEG-functionalized and conjugated with antibodies for AD biomarkers recognition. Each type of immune-AuNPs undergoes individual detection events, resulting in an LSPR shift at a distinct extinction peak (λ_{max}), enabling simultaneous analysis without the need for additional separation and identification efforts. As the measurement procedure was like bar-code scanning, the authors described it as a shape-coded biosensor [113].

Song et al. devised DNA-assembled advanced plasmonic architecture (DAPA) and established a DAPA-based plasmonic biosensor for detecting exosomal miRNAs associated with AD, such as miRNA-125b, miRNA-15a, and miRNA-361. The DAPA nanoarchitecture comprises seed particles of three spherical AuNPs functionalized with ssDNA. These AuNPs are interconnected via hybridization of ssDNA strands, creating two nanogaps (2 nm) between each pair of particles. Consequently, a rod-shaped structure is formed, leveraging nanogaps to focus incident light and generate hot-spots, thereby amplifying the overall electromagnetic field energy and plasmonic coupling effect. Detection of miRNAs is accomplished on the DAPA surface using capture DNA and locked nucleic acid probes to form complexes with target miRNAs. This interaction induces a red shift in the LSPR peak, with its amplitude enhanced by the presence of nanogaps in the DAPA structure, enabling attomole-level sensitivity [114].

Chang et al. integrated the strategy of fiber optic nanogold-linked sorbent assay (FONLISA) and DNA ligation specificity, developing a fiber optic particle plasmon resonance (FOPPR) biosensor for the assessing of *ApoE* genotyping in DNA extracts from human blood [115]. This methodology uses two probes that are complementary to target ssDNA. One probe is biotinylated, while the other is immobilized on dual-functional gold-iron oxide core-satellite hybrid nanoparticles (HNPs). When the target ssDNA is present, these probes form pairs through ligation, which can be detected with the assistance of HNPs. The HNPs serve as both plasmonic signal reporters and magnetic carriers for purifying ligated samples. The ligated products are subsequently captured by streptavidin-functionalized optical fibers, forming a sandwich-like complex on the fiber surface. This results in a change in the transmitted light intensities. The magnitude of this difference allows for the discrimination of six *ApoE* genotypes, with excellent performance in terms of minimal sample consumption (20 μL of blood), sensitivity, and specificity [116].

3.1.3. Surface plasmon resonance

Surface plasmon resonance (SPR), akin to LSPR, involves the oscillation of surface plasmons induced by incident light at specific angles. However, unlike LSPR, this phenomenon is not confined to nanostructures but distributed across the metal surface. In SPR-based biosensors, biomolecular interactions on the sensor surface lead to changes in reflectivity, angle, or wavelength over time. The intensity of these changes is proportional to the target concentration and is measured for analysis [90,92].

Zheng et al. identified two aptamers with specificity for both oligomeric and fibrillar forms of $A\beta_{40}$ aggregates, showing distinct recognition patterns via single-molecule force spectroscopy [117]. Accordingly, they developed an SPR-based dual-aptasensor to detect and differentiate between the two types of $A\beta_{40}$ aggregates in CSF. This sensor is created by immobilizing one aptamer on an Au film surface and the other on AuNPs. The utilization of two aptamers helps to avoid steric hindrance during recognition and enhances the selectivity and sensitivity of biosensing. The presence of $A\beta_{40}$ oligomers or fibrils results in changes in SPR resonance angle shift, reflecting the quantity of $A\beta_{40}$ aggregates [118]. Špringer et al. employed two types of antibodies and functionalized AuNPs for detecting tau-amyloid β complexes (tau-Aβ complex). In a sandwich-designed assay, when the target tau-Aβ complex passes over the SPR chip surface immobilized with tau antibodies, it is captured by its tau part and subsequently binds to the biotinylated Aβ antibody by its Aβ part. Finally, the biotinylated end of the Aβ antibody binds to streptavidin-functionalized AuNPs (S-AuNPs), enhancing the SPR signal response rather than providing a colorimetric signal. This increases the mass on the metal chip surface, causing complex changes in the refractive index of the sensor chip, which are amplified by the binding of S-AuNPs. Consequently, under incident light, the binding events of tau-amyloid β complexes on the sensor chip cause a wavelength shift at the SPR dip, which is used as the sensor response for quantifying the target protein complexes [119].

To enhance the sensitivity of SPR biosensors, a stronger electric field on the metal surface is required, which can be achieved by incorporating non-plasmonic graphene-based materials. For instance, graphene and graphene oxide (GO) are two-dimensional materials known for their charge

transfer capability, high surface area for biomolecule binding, and ease of fabrication. These materials can be combined with metallic plasmonic materials to augment the electric field and improve sensitivity to changes in refractive index [120]. Building on this concept, Nangare et al. developed a GO-SPR biosensor for detecting $A\beta_{42}$. In addition to enhancing specificity and sensitivity, they employed the layer-by-layer (LbL) technique and assembled nanomaterials to immobilize multiple antibodies for target recognition. The LbL assembly consisted of AgNPs coated with layers of chitosan (CS) and polystyrene sulphonate (PSS) applied sequentially, with antibodies affixed to the outer layer (AgNPs–CS–PSS-CS@anti-Aβ). This assembly was then deposited onto the activated GO surface of the SPR biosensor. Upon capturing $A\beta_{42}$ by the antibodies, the binding events induced changes in the SPR signal, which were amplified by the coupling of GO and LbL assemblies, facilitating the detection of $A\beta_{42}$ [121].

Optical fiber-based SPR sensors have been developed for the detection of AD biomarkers [122–125]. These sensors utilize total internal reflection within the optical fiber to generate an evanescent field, while the fiber surface is coated with plasmonic metallic materials, enabling the induction of SPR with enhanced sensitivity. Furthermore, this type of SPR sensor is compact, adaptable to various materials and mechanical configurations, and suitable for remote sensing, making it a potential candidate for point-of-care testing [126,127]. Nu et al. demonstrated an SPR fiber sensor for serum Tau detection. They replaced the fiber cladding with Cr/Au coating and utilized a light source at 632.8 nm to achieve optimal SPR conditions. Binding events cause changes in fiber output power for multiplexed detection of t-tau and p-tau. The signal change increases with increasing Tau concentration, resulting in a nonlinear fitting with two exponential functions. Additionally, as the metal layer is coated with an elliptical cross–sectional profile, the evanescent wave attenuates in different directions, allowing more penetration into the metal layers to excite a greater number of surface plasmons. This enhances sensitivity compared to a uniform metal layer [124,128]. Khatri et al. designed a U-shaped SPR optic fiber biosensor to distinguish between monomeric and aggregated fibril forms of αSyn. The U-shaped optic fiber was manufactured by exposing the decladded region to a butane flame, applying sufficient force on both sides of the fiber, and bending it into a U-shape with a radius of 1.5 mm. The outer side of the uncladded U-bent section was then immobilized with AuNPs and further coated with CS, serving as the probe for αSyn fibrils. CS selectively binds to αSyn fibrils but not monomers, leading to absorbance changes at 530 nm that can be utilized to detect different forms of αSyn in mixtures [122]. The U-shaped configuration alters the light propagation along the fiber compared to a straight fiber, enhancing sensing sensitivity. The bending mechanical force causes the refractive index distribution in the fiber core to be uneven, with more significant refractive index changes occurring as the bend radius decreases [128,129]. Additionally, at the outer side of the U-bend, higher-order modes attenuate, and the penetration depth of the evanescent field increases, which in turn stimulates more localized surface plasmons of the AuNPs, resulting in stronger signals [127].

A dual-channel SPR sensor chip based on enzymatic cleavage reactions was established for *ApoE* genotyping without DNA amplification. Developed by Yi et al., this method utilizes a gold-filmed chip with immobilized complementary DNA probes, one end of which is modified with biotin, enabling recognition by streptavidin to amplify SPR signals. Depending on the SNP of the *ApoE* gene, the target gene fragments can be either single-base mismatch (GTGC) or complementary (GCGC) to form a duplex with the anchored probes. The latter duplex pairs are then cleaved by the restriction enzyme HhaI, resulting in a reduction of biotin-streptavidin recognition, followed by differential SPR signals for *ApoE* genotyping in humans [130].

Biolayer interferometry (BLI) is a robust optical biosensor capable of detecting various types of analytes. Functionally, BLI takes the form of a disposable optical fiber-based biosensor and operates in a Dip-and-read format. The biolayer interface at the end of the fiber is dipped into the sample well to interact with target molecules [131]. As the incident white light travels down the optic fiber to the end, the internal and external surfaces of the biolayer reflect the light back to spectrophotometers asynchronously due to distance differences, establishing an optical interference pattern [131,132]. The pattern is plotted with the reflected wavelength on the x-axis and relative intensity on the y-axis. In the presence of analytes, binding events change the thickness of the biolayer and increase the propagation length of light, resulting in a wavelength shift in the interference pattern. Since the shift is associated with the size, affinity, and amount of bound analytes, BLI can detect the number of analytes in real-time or monitor dissociative events over time by measuring this shift [131–133]. Ziu et al. developed a BLI-

based aptasensor for the Tau protein (Tau441) by immobilizing a biotinylated aptamer on the streptavidin interface as a capture probe. This aptasensor marks the first BLI application in AD biomarkers and demonstrates selectivity over Aβ and αSynwhen applied to fetal bovine serum [134].

SPR imaging (SPRi) is an extension technique of SPR, which combines the properties of SPR with microarray imaging, enabling high-throughput and simultaneous analysis of multiple reactions [135]. Gao et al. utilized $A\beta_{42}$-specific binding material, AD peptoid 3 (ADP3), along with SPRi technique to develop an SPR nanosheet sensor for $A\beta_{42}$ detection in plasma and serum. The nanosheet sensor was composed of amphiphilic self-assembling peptoids immobilized on a functionalized gold chip surface, with ADP3 inserted and exposed as a loop on the surface to mimic $A\beta_{42}$ antibodies. The presence of $A\beta_{42}$ would be recognized by ADP3 loops, resulting in changes in the RI on the chip surface, which are recorded to reflect the binding events on the surface [136].

Plasmonic interferometry, a nano-plasmonic biosensor introduced by Feng et al., employs a nanoscale groove-slit-groove design on a metal surface, as shown in Fig. 3. This innovative technique combines the properties of surface plasmon polaritons in gold with light interference to detect both SPPs excitation and RI changes caused by compositions near the surface [137]. Unlike typical SPR or LSPR, plasmonic interferometry overcomes limitations such as the need for specific frequencies for resonant scattering and extinction production. With its broadband operations, allowing simultaneous detection of RI changes at multiple wavelengths, wide-angle excitation feasibility, and miniaturized sampling volume and sensing area, plasmonic interferometry emerges as a high-throughput device for biosensing [137]. Li et al. employed this technique with antibody-surface functionalization and successfully detected TREM2 in CSF, highlighting the potential of this technical approach for developing other immunoassays in the future [138].

In summary, SPR and LSPR-based biosensors offer label-free detection, real-time response, and exceptional sensitivity in the picomolar/femtomolar range. As outlined in Table 3, these methods are capable of detecting and distinguishing various AD biomarkers, including but not limited to Aβ species, tau proteins, *ApoE* genotypes, and miRNAs. Many of these biosensors incorporate recognition elements to enhance selectivity and mitigate non-specific binding. Additionally, they utilize diverse nanostructures, non-plasmonic materials, optical fiber

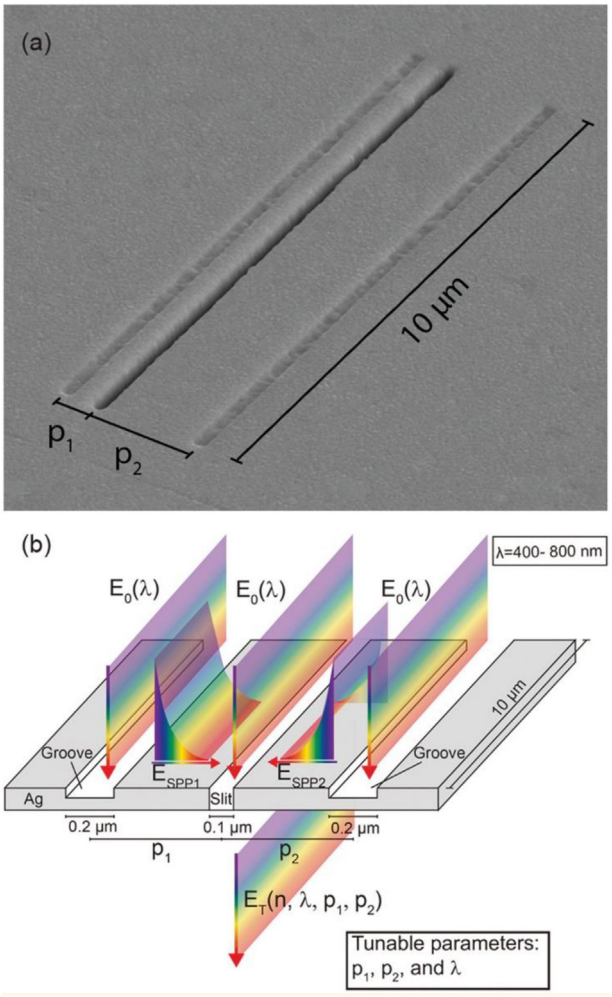

Fig. 3. Graphical illustration of a plasmonic interferometer with (a) scanning electron microscopy micrograph of a groove-slit-groove design on the metal surface, and (b) schematic working principle. Reprinted with permission from Nanoscale Plasmonic Interferometers for Multispectral, High-Throughput Biochemical Sensing (Ref [137]). Copyright 2012 American Chemical Society.

configurations, two-dimensional arrays, and interferometric principles to achieve miniaturization, simplification, high-throughput capabilities, and multiplex analysis. These advancements serve as inspiration for the development of biosensors targeting other analytes.

Based on the preceding discussion, colorimetric sensors are essential techniques widely employed for detecting AD biomarkers. These sensors exploit the principle of color change and are typically constructed using various components such as chromogenic substrates, peroxidative enzymes, metallic, and composite nanomaterials. Offering advantages of label-free detection, naked-eye visibility, and high sensitivity in biological samples, these technologies have demonstrated specificity for target biomarkers and applicability in simulated or

Table 3. Nanomaterial-based SPR/LSPR sensors for AD biomarkers.

Nanomaterials	Biomarkers	Recognition element	Limit of detection	Sample	References
Au nano-urchins	$A\beta_{42}$	–	–	–	[112]
AuNPs, AuNRs	$A\beta_{40}$, $A\beta_{42}$, Tau protein	Antibody	34.9 fM for $A\beta_{40}$ 26 fM for $A\beta_{42}$ 23.6 fM for Tau protein	Mimicked blood	[113]
DADP, gold nanomaterials	miRNA-125b, miRNA-15a, and miRNA-361	ssDNA	10.54 aM for miR-125b, 13.53 aM for miR-15a, 11.10 aM for miR-361	Human blood	[114]
AuNPs	$A\beta_{40}$ aggregates	Aptamer	0.2 pM for $A\beta_{40}O$, 0.05 pM for $A\beta_{40}$ fibrils	Human CSF	[118]
AuNPs	Tau–Aβ complex	Antibody	1 pM	Human CSF	[119]
AgNPs–CS–PSS-CS@anti-Aβ, GO	$A\beta_{42}$	Antibody	1.21 fg/mL	Rat blood and saliva	[121]
Au/Cr coated fiber	t-tau, p-tau	Antibody	2.4 pg/mL for t -tau, 1.6 pg/mL for p-tau	Human serum	[124]
AuNPs	α-synuclein		–	–	[122]
Gold-iron oxide core-satellite HNPs	*ApoE* gene	ssDNA	16-38 fM	Blood DNA extracts	[116]
Gold film	*ApoE* gene	ssDNA	10-50 fM	Blood DNA extracts	[130]
–	Tau441	Aptamer	6.7 nM	Fetal bovine serum	[134]
Peptoid nanosheet	$A\beta_{42}$	ADP3 loop	1 pM	Human blood	[136]
Gold layer	TREM2	Antibody	–	–	[138]

Abbreviations: Ach: acetylcholine, AchE: acetylcholinesterase, ADP3: AD peptoid 3, AgNPs: silver nanoparticles, anti-Aβ: Aβ antibody, AuNPs: gold nanoparticles, AuNRs: gold nanorods, CS: chitosan, DADP: DNA-assembled advanced plasmonic, GO: graphene oxide, HNPs: hybrid nanoparticles, PSS: polystyrene sulphonate.

real biological specimens. Thus, colorimetric sensors hold significant promise for the diagnosis and monitoring of AD and are poised to continue playing a pivotal role in future research and applications.

3.2. Nanomaterial-based fluorescent sensors

Nanomaterials can be applied as a fluorescent indicator, quencher, and carrier in the fluorometry detection strategy (shown in Fig. 4). Compared to

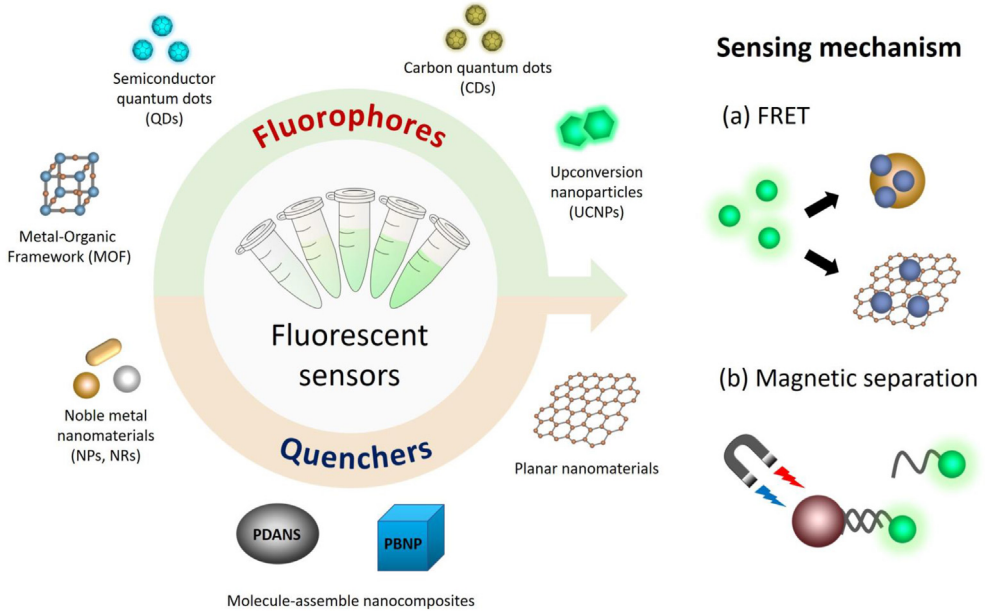

Fig. 4. Fluorometric strategies for AD biomarkers based on nanomaterials which were constructed as fluorophore or quencher. (a) Fluorescent sensor based on FRET-induced quenching. (b) Fluorescent sensor based on magnetic separation-induced signal decline.

traditional fluorophores such as fluorescein amidites (FAM), cyanine-5 (Cy5) and so on, fluorescent nanomaterials, such as quantum dots (QDs) [139], upconversion nanoparticles (UCNPs) [140], and MOF [141], possess unique optical properties like large Stokes shift, ease of modification and controllable emitting wavelength. These properties provide more flexibility to establish diverse fluorometric methods. On the other hand, the application of nanomaterials as a quencher in a fluorometric method is also useful to enhance the performance due to the high extinction coefficient or high interaction surface, which facilitates the electron transfer, especially noble metal nanoparticles and GO [142,143]. Other nanomaterials, such as Prussian blue nanoparticles (PBNPs), polydopamine nanoparticles (PDANS) and transition metal nanosheets [144–146], were also established as a quencher for the development of biosensing methods. Furthermore, nanomaterials, such as magnetic nanoparticles (MNPs), can serve as carriers, capable of functionalizing recognition elements and providing diverse detection mechanisms by magnetic properties [147]. Table 4 summarizes the nanomaterial based fluorescent sensors used for AD biomarkers detection. It includes nanomaterials, recognition elements, limit of detection, and sample matrix.

Table 4. Nanomaterial-based fluorescent sensors for AD biomarkers.

Nanomaterials	Biomarkers	Recognition element	Limit of detection	Sample	References
(1) GSH-capped CdTe QDs (2) AuNPs	AβO	PrP (95–110) peptide	0.2 nM	–	[149]
(1) $BaYF_5$:Yb,Er UCNPs (2) MNPs	AβO	Aptamer	36 pM	aCSF	[151]
PDANS	AβO	Aptamer	12.5 nM	–	[176]
GO	AβO	Aptamer	20 pM	Exosome	[181]
MNPs	$Aβ_{42}$ Tau441 p-tau 181	Antibodies 12F4 for $Aβ_{42}$ BT2 for Tau441 AT270 for p-tau181	38 fg/mL for $Aβ_{42}$ 197 fg/mL for Tau441 165 fg/mL for p-tau181	Human CSF	[31]
$CuInS_2$/ZnS QDs	Tau protein	Aptamer Antibodies TYR-anti-Tau	10 pM	Human serum	[156]
CDs@Eu/GMP ICP nanoparticles	Aβ monomer	Cu^{2+}	0.17 nM	AD mice brain tissue	[166]
AuNPs	$Aβ_{40}$ $Aβ_{42}$	SEA-SC2 (fluorescent molecule)	–	aCSF	[180]
PBNPs	AβO	Aptamer	1 nM	aCSF Human CSF	[175]
MoS_2 NSs	AβO	Aptamer	3.1 nM	AD mice brain tissue	[173]
L-MOF AuNPs	AβO	Aptamer	0.3 pM	Human serum	[150]
L-MOF-armored-anti-DNA antibody	AβO	Aptamer	0.4 pg/mL	Human serum	[169]
ThT@Er-MOF	Presenilin 1 Aβ protein	Spilt SSODN-P1 & P2 –	0.517 pM for presenilin 1 0.142 nM for Aβ protein	aCSF	[170]
TAMRA-labeled substrate strand-AuNPs	AβO	Aptamer	22.3 pM	Living cell Mice brain	[177]
FAM-dsDNA-GO	AβO	Aptamer	0.1 nM	Human CSF	[179]
UCNPs MOF	AβO	H-USM (Zn^{2+})	28.4 pM	–	[171]
CdSe/CdS/ZnS QDs AuNRs@PDA	AβO Tau protein	AβO aptamer-QDs_{625} Tau aptamer-QDs_{665}	50 pM for AβO 20 pM for Tau protein	Human serum	[157]
NCDs	p-tau231	Aptamer	3.64 ng/mL	–	[148]
NCDs BP nanosheets	AβO	Antibodies	83 pg/mL	Artificial serum	[165]

Abbreviation: Aβ P: aptamer for Aβ42, Ach: acetylcholine, AchE: acetylcholinesterase, aCSF: artificial cerebrospinal fluid, AuNRs@PDA: polydopamine-capped gold nanorods, BP: black phosphorus, CdSe/CdS/ZnS QDs: CdSe/CdS/ZnS core/shell/shell quantum dots, Er-MOF: metal–organic framework $[Er(L)(DMF)_{1.27}]_n$, GMP: 5′-guanosine monophosphate disodium, GSH: glutathione, H: hairpin probe, H-USM: highly doped upconversion nanoparticles-SiO_2@MOF microspheres, ICP: infinite coordination polymer, L-MOF: luminescent metal–organic framework, MNPs: Fe_3O_4 magnetic nanoparticles, MoS_2 NSs: molybdenum disulfide nanosheets, NCDs: nitrogen-doped carbon dots PBNPs: prussian blue nanoparticles, SSODN: part of the presenilin 1 gene, Spilt SSODN-P1 & P2: DNA complementary pair sequence with SSODN 1 & 2, Tau P: aptamer for Tau441 and p-tau181, PDANS: polydopamine nanospheres, ThT: thioflavin T, TYR: tyrosinase.

3.2.1. Nanomaterials as a fluorescent indicator

The application of nanomaterials such as QDs [148,149], MOF [150], and UCNPs [151] as fluorescent indicators to develop sensors for detecting biomarkers of AD is summarized here. QDs are the most commonly used nanomaterials-based fluorescent indicator. The QDs can be divided into two categories: semiconductor QDs and carbon-based QDs (CDs) [152,153]. The emitted wavelength of QDs is tunable by manipulating the size of QDs according to the quantum confinement effect [154,155]. The changing size of QDs can influence the discretization of electronic energy states, which induces the confinement of electrons and holes by the conduction and valence bands. With the property of QDs, the detected fluorescent signal can be flexibly designed, depending on the requirement of developed analytical methods. For semiconductor QDs, they were widely applied in the development of optical biosensing methods with diverse fabrication strategies, such as CdTe QDs [149], $CuInS_2$/ZnS QDs [156], CdSe/CdS/ZnS QDs [157]. A critical drawback of QDs is their poor solubility in water, which can make them incompatible with biosensor applications. Modifying the surface of QDs with hydrophilic functional groups is an ideal solution to overcome this problem. Xia et al. developed a glutathione-capped CdTe QDs sensor based on the inner filter effect (IFE) from AuNPs for the detection of AβO [149]. The non-irradiation energy conversion of IFE provided a flexible quenching of QDs by AuNPs upon the overlapping of emission and absorbance of QDs and AuNPs, respectively [158]. The modification of glutathione onto the surface of QDs as a stabilizer can enhance water-solubility and biocompatibility [159]. In addition to ligand functionalization, a surface-coating of QDs with a layer, such as ZnS, is also feasible to coordinate the compatibility between QDs and aqueous environment. Notably, the surface passivation by ZnS can also enhance the photoluminescence of QDs induced by band-edge recombination due to the suppression of deep trap emission [160]. The deep trap, the band gap in the middle of exciton absorption/emission band, will trap exciton and cause the quantum yield to decrease. With a ZnS shell on the surface of QDs, the energy band gap can be broadened, suppressing deep trap emission and allowing more electrons to return to the ground state [161]. It allows semiconductor QDs to possess outstanding optical characteristics that can enhance their photoluminescence under extra passivation by a surface-coating process. In addition, ligand functionalization or exchange can be achieved in the semiconductor QDs system, allowing them to be applied in various detection strategies [162]. Core/shell QDs, with their optical properties and ligand exchange, were used as fluorescent indicators for biosensing. Lu et al. developed an aptasensor for the simultaneous detection of AβO and tau protein by two kinds of CdSe/CdS/ZnS QDs with different emission wavelengths by an identical excitation and applied polydopamine-capped gold nanorods as the quenching medium [157]. Additionally, a strategy was devised for the functionalization of quantum dots with redox-active biomolecules. Chen et al. developed a sandwich immune-aptasensor for the detection of tau protein. A dopamine-functionalized $CuInS_2$/ZnS QDs were used as the signal indicator, and the tau-antibody was functionalized with tyrosinase. The dopamine on the QDs can transform to be dopamine quinone due to the catalytic oxidation by tyrosinase. The fluorescence of QDs will be quenched by the dopamine quinone, which serves as an electron acceptor [156].

The optical properties of CDs are similar to those of semiconductor QDs. The surface passivation of CDs induced the energy trap and emitted a photoluminescence [163]. Yet, the synthesis of QDs can be achieved by the carbonization of natural organic materials and can be easily manipulated in the aqueous environment, such as hydrothermal synthesis [164]. Thus, fabricated CDs are more environmentally friendly than metal QDs and more appealing to be applied in biosensing strategy without additional hydrophilic modification. For instance, Phan et al. used citric acid monohydrate as a carbon source and PEI1800 as a nitrogen source to synthesize nitrogen-dopped CDs (NCDs), which possess positive-charged surface and pyridine-type fluorophore intermediates on the surface [148]. The positively charged surface of NCDs allowed nucleic acid, such as aptamers, to attach onto their surface by electrostatic interaction, which can also induce fluorescence resonance energy transfer (FRET), causing fluorescence quenching from NCDs. They applied this mechanism to develop an aptasensor for the detection of p-tau231 upon the detachment of aptamer out of NCDs. When p-tau231 was introduced, it bound to the aptamer, causing the NCDs to be released and resulting in the recovery of fluorescence. Besides, the NCDs can also be implemented a surface functionalization with antibodies so as to construct an immune-based biosensor [165]. On the other hand, CDs can also serve as an antenna ligand to assist the self-assembly of europium (Eu^{3+}) and 5′-guanosine monophosphate disodium (GMP) to form CDs@Eu/GMP infinite coordination polymer nanoparticles which encapsulated CDs inside the Eu/GMP network. This can be attributed to the

abundant functional groups of CDs (-COOH and $-NH_2$), which allow for the interaction of coordination. The as-formed nanoparticles can be utilized to detect Aβ monomer in a detection environment with cupric chloride to provide Cu^{2+}, which can coordinate with Aβ monomer. The competitive mechanism of Cu^{2+} against Eu^{2+} for the coordination to CDs disrupted the antenna effect of CDs, leading to the decline of fluorescence, and the stronger interaction of Aβ monomer against Cu^{2+} can recover the fluorescence [166]. Compared to semiconductor QDs, CDs have superior biocompatibility and lower toxicity than semiconductor QDs. The manufacture of carbon dots is flexible, allowing for diverse configurations from carbon and ligand sources. However, their actual composition and surface characteristics are challenging to identify.

Other fluorescent nanomaterials, such as MOFs and UCNPs, also possess appealing properties applicable to sensor development. Unlike small QDs or CDs less than 10 nm, MOFs and UCNPs have larger dimensions, providing more capacity to implement surface modification. MOFs are geometrically structural porous crystalline composed of metal clusters, organic ligands (linkers), and guest molecules. MOFs possess a luminescent property attributed to the linker excitation, which performs a charge transfer with metal clusters. In addition, the π-π stacking interaction between adjacent aromatic structures in MOFs provides a large Stokes shift in emission [167]. UCNPs were mainly composed of rare earth elements, including the lanthanide (Ln) family and yttrium (Y) with abundant energy level which can implement intra-configurational transitions. These traits allow UCNPs to emit luminescence under near-infrared excitation [168]. These nanomaterials with luminescent properties can be feasibly utilized in the development of sensors by modification of recognition elements [151] or direct surface interaction upon intermolecular force and electrostatic attraction with recognition elements [150,169]. In the practical application, the optical property of MOF allowed researchers to develop various detection mechanisms [150,169,170]. For instance, Wang et al. construct a multifunction thioflavin T (THT)-embedded Er-MOF sensor for the detection of various biomarkers for AD, including Aβ, acetylcholine, and the gene of presenilin 1. The conjugated structures in MOF provide hydrophobic and π-π stacking interactions against protein or DNA sequences. These surface interactions can further affect the emissive ability of MOF. Additionally, the embedded THT provides selectivity of Aβ, making MOF a suitable candidate for developing diverse biosensing methods [170]. On the other hand, the MOF technique can also be combined with the UCNP technique. Fang et al. developed optically trapped highly doped upconversion nanoparticles, SiO_2@MOF microspheres (H-USM), which wrapped BHQ-1 inside the structure of MOF. The wrapped BHQ-1 can quench the luminescence of UCNPs via luminescent resonance energy transfer. The method was used to detect AβO by the interaction between AβO and the Zn^{2+}-fabricating MOF, attributed to the high affinity of histidine (His), glutamate (Glu), and aspartic acid (Asp) of Aβ peptide against Zn^{2+}. AβO can induce the disassembly of MOF, and subsequently, BHQ-1 molecules will be released out of microspheres. Eventually, the luminescence of UCNPs can be recovered, and the changing signal can be utilized to quantify the levels of AβO [171].

3.2.2. *Nanomaterials as a quencher*

AuNPs are commonly used as a quencher due to a high extinction coefficient and a broad absorption spectrum, which enables them to effectively quench fluorescence by overlapping with the emission of common fluorophores [142,172]. Another common quencher, GO, is a planar nanomaterial with abundant aromatic structures composed mostly of sp^2-hybridized carbon atoms. GO provides the property of π-π stacking interaction, which can attract substances with aromatic structures and quench fluorescent indicators through electron transfer [143]. Similar to GO, the planar structural transition metal nanosheets, such as black phosphorus nanosheets and MoS_2 nanosheets [165,173], were also regarded as appealing quenchers in the development of analytical methods. These planar nanomaterials also possess electron transfer properties that facilitate fluorescence quench. Attributed to their charged property, the adsorption of recognition elements can easily be achieved by the van der Waals force and intermolecular force [174].

Other nanomaterials, such as PBNPs and PDANS, also possessed the property to quench fluorescence. Fe^{3+} and Fe^{2+} ions can quench fluorescent indicators on PBNPs by attracting negatively charged substances to the surface, facilitating energy transduction [175]. On the other hand, PDANS possessed the structure of aromatic polydopamines which provided intermolecular force, such as π-π stacking interaction and hydrogen binding against positive charged or aromatic substances. When fluorescent indicators are close to PBNPs, the fluorescence can be quenched due to the broad absorption spectrum [176].

In the application of these nanomaterials with quenching properties, researchers can functionalize recognition elements onto the surface of AuNPs

[150,177] or GO [178,179], such as nucleic acids (aptamer) and antibody. In addition to surface functionalization of recognition elements onto nanomaterials, several detection mechanisms were designed to directly adsorb recognition elements onto the surface of nanomaterials with quenching properties by intermolecular force or electrostatic attraction, including small molecules [180], peptides [149], nucleic acids [157,173,175,176,181] and antibody [165]. Relying on altering the distance between the fluorescent indicator and nanomaterials with quenching properties, in the presence or absence of a target, the changing fluorescent signal can be utilized to quantify the level of a target.

3.2.3. Nanomaterials as a carrier

MNPs were the most used nanomaterials as carriers that could load recognition elements. Different from the quenching property, such as FRET or dipole–dipole coupling, the changing fluorescent intensity can be attributed to eliminating magnetic carriers in the detection environment by an external magnetic field. Take the research from Jiang et al. as an example, they established an aptamer complementary DNA-functionalized BaYF5:Yb,Er UCNPs coupled with a magnetic separation technique through aptamer-functionalized MNPs for the detection of AβO [151]. AβO can resist the hybridization between sequences on UCNPs and MNPs when AβO interacts with aptamers on the surface of MNPs. A distinct fluorescent signal can be obtained in the presence of AβO. In contrast, a decline signal can be observed in the absence of AβO due to the elimination of UCNPs from the detection system by MNPs.

In addition to the magnet-assisted separation, MNPs can also serve as carriers with diverse shapes, which can be used to distinguish different analytes when these carriers are functionalized with recognition elements for specific targets. For example, Chan et al. developed two magnetic nanocomposites to detect $A\beta_{42}$, Tau441, and p-tau181 in visualization. For Tau441 and p-tau181, sphere-shaped magnetic nanocomposites were fabricated and conjugated with Tau441 or Tau181-specific capture antibody; for $A\beta_{42}$, magnetic Janus rods were constructed and functionalized with $A\beta_{42}$-specific capture antibody. To enhance the sensitivity, Chan et al. utilized aptamers of Tau181 and $A\beta_{42}$ coupled with the technique of HCR [182]. By using a tailor-made fluorophore, called SPOH, which can bind to double-strand DNA generated from the HCR, a fluorescent image exhibiting the dispersion of different morphological magnetic carriers with $A\beta_{42}$, Tau441, and p-tau181 can be obtained and further can be quantified the levels of analytes [31].

Recently, the utilization of fluorescent or quenching indicators has gradually turned from conventional molecules to optical nanomaterials. Optical nanomaterials can be further implemented through surface modifications or functionalization. The modification of nanomaterials allows researchers to refine the sensing performance, which can't be effectively manipulated in the context of a traditional fluorometric method by optical molecules, such as reduction of nonspecific adsorption, recognition of targets, providing better reaction space, combination with signal amplified techniques and so on. Optical nanomaterials which not only serve as the source of detection signal but also provide other functions, diverse detection mechanisms of fluorometry can be achieved. The high flexibility of constructing a fluorescent sensor allowed researcher to design an appropriate method according to their research strategy. However, some functional fluorescent indicators are hard to fabricate or have a complicated manufacturing process, including synthetic and functionalization procedures. Even if they possessed outstanding optical properties or multiple functions, the drawback of manufacturing inevitably limits the practical application of these fluorescent nanomaterials. The reliability and applicability will be greatly improved if the process of manufacturing these nanomaterials can be simplified. Such an improvement also benefits the quality control of fluorescent nanomaterials from batch to batch.

3.3. Surface-enhanced Raman scattering

Raman scattering is the inelastic scattering of radiation ascribed to molecules' vibration, namely the Raman effect. However, a weak Raman effect sometimes occurs and leads to low sensitivity. This drawback limits the utilization in the development of analytical methods for trace amounts of analytes. Fleischmann group first proposed an improved strategy for Raman scattering, also known as SERS. While conducting experiments, they discovered that adsorbing pyridine on rough silver surfaces led to an unexpectedly large Raman signal [183]. According to their observations, the increased intensity can be obtained due to the enhanced electromagnetic effect and chemical effect, induced by localized surface plasmons from metals on a nano-scale and the adsorption of molecules onto the surface of metals, respectively [184]. The region of magnified electromagnetic field by the effect of LSPR was also known as “hot spots” [185]. Many researchers have

investigated the shape and size of plasmonic nanomaterials to obtain an optimized amplified intensity of SERS. When the distance of immobilized nanomaterials gets into close proximity but are not in touch with each other, the electromagnetic field of "hot spots" can be acquired, which provides the highest enhancement of Raman scattering. The maximum enhancement factor of the Raman signal is approximately ten orders of magnitude [186]. The breakthrough of SERS successfully became prevalent in the development of sensitive analytical methods. SERS has been successfully applied in assays requiring high sensitivity for AD biomarkers. The SERS techniques developed to detect AD biomarkers have been summarized in Table 5, and the schematic diagram is shown in Fig. 5.

Attributed to the SERS spectra exhibition, the changing formation of Aβ during self-aggregation can be observed by the changing of dominant wavelength on α-helix and β-sheet structure [187]. In addition to the qualification of Aβ conformation, the SERS technique is also eligible to quantify biomarkers of AD. In the construction of SERS-active plasmonic nanomaterials, researchers have developed various morphologies of nanomaterials to enhance electromagnetic fields. For instance, Wang et al. established chiral triangular nanorings (chiral Pt@Au TNRs) for the detection of $A\beta_{42}$ monomers and fibrils [188]. The Raman scattering of $_{D}$-Pt@Au TNRs after interacting with analytes was significantly enhanced, attributed to surface-enhanced Raman scattering-chiral anisotropy (SERS-ChA) [189]. Additionally, the conformation of $A\beta_{42}$ monomer and fibrils can also be discriminated and quantified from the vibrational information of Raman spectra by the transformation of Raman peaks from the α-helical structure to the β-sheet structure [188]. Moreover, Yu et al. developed a graphene-gold hybrid plasmonic platform with a pyramid structure which concentrated hot spots and facilitated the SERS enhancement. This platform achieved a high detection efficiency with a detection limit of 1 aM [190].

In addition to the investigation of the morphology of plasmonic nanomaterials, the substrate underneath them can also influence Raman enhancement performance by providing charge transfer [191,192]. The substrate structure for SERS can be divided into rigid and flexible substrates. Generally, a rigid substrate is the most commonly applied substrate for the development of SERS-based sensors, such as indium tin oxide (ITO) [193], graphene [190], GO [194], gold pellet [195], laser-induced deposition (LID) [196]. For detecting $A\beta_{42}$, Yu et al. used a single layer of graphene loaded with a pyramid-shaped gold structure [190]. Graphene enhances the Raman signal by transferring charge through π-π stacking between analytes and graphene [197]. Furthermore, graphene also possesses an intrinsic Raman signal, which can serve as an internal standard for the sensor [190]. Yu et al. also utilized GO to immobilize Fe_3O_4 nanoparticles, avoiding self-gathering and enhancing biocompatibility and dispersion [194]. Eremina et al. conducted an LID experiment by immersing the coverslip in a solution of silver benzoate in methanol and illuminating it with a laser source. The laser-induced chemical reaction can reduce metal ions to metals, and metals can further precipitate on the substrate surface with high adhesion [198]. An AgNPs-immobilized LID (AgNPs/LID) was fabricated and utilized to construct a SERS-based sensor for the detection of Cu^{2+} assisted aggregated $A\beta_{42}$ ($CuA\beta_{42}$) which can acquire a limit of detection down to 1.5 pM by a 633 nm laser [196]. In addition, researchers have investigated the use of a flexible SERS substrate due to its advantageous properties of being easily prepared and scalable [191,199]. Jaiswal et al. fabricated a polyacrylonitrile nanofibrous mat with a purine-based ligand via electrospinning, then functionalized it with AgNPs (P_3/AgNPs) as a SERS sensor for detecting $A\beta_{42}$ and human insulin. The purine-based ligand possessed non-covalent interaction with peptide analytes and could bind AgNPs due to nitrogen centers in its heterocyclic structure. With the cooperation of surface interaction of AgNPs and non-covalent interaction between analytes and purine-based ligand, the fabricated P_3/AgNPs SERS sensor acquired enhancement factors of 3.1×10^{12} and 6.6×10^{12} for $A\beta_{42}$ and human insulin with detection limits of 76 aM for $A\beta_{42}$ and 26 aM for human insulin [200]. Likewise, Eremina et al. utilized a uniform distribution of AgNPs on the CS substrate, achieved through a colloidal suspension, to form AgNPs/CS substrate in developing a SERS sensor. This SERS sensor was applied to differentiate between amyloid aggregates and monomers. Meanwhile, the sensor can detect Zn^{2+}-assisted aggregated $A\beta_{42}$ ($ZnA\beta_{42}$) with a limit of detection of 1.5 nM for $A\beta_{42}$ aggregates using a 532 nm laser [196].

SERS-based methods possess the property of identifying targets with specific Raman fingerprint information attributed to intrinsic molecular vibration. However, these methods may yield false-positive signals, especially when detecting analytes in complex matrices. Additionally, the specificity of the developed methods may be a dilemma, especially for those targets with compositions similar to their analogs. To overcome this problem, some researchers utilized recognition ligands such as small molecules, antibodies, or aptamers on the surface of

Table 5. Nanomaterial-based SERS sensors for AD biomarkers.

Nanomaterials	Biomarkers	Recognition element	Limit of detection	Sample	References
Non-antibody or aptamer					
Au nanoshell	AβO	Sialic acid-modified Au nanoshell	1 pM	–	[201]
Graphene–gold hybrid plasmonic platform	$A\beta_{42}$	–	1 aM	Human plasma	[190]
AuNPs	$A\beta_{42}$	RB-AuNPs	–	Mouse brain slice	[202]
Chiral Pt@Au TNRs	$A\beta_{42}$ monomers $A\beta_{42}$ fibrils	$_D$-Pt@Au TNRs	45 fM for $A\beta_{42}$ monomer 4 fM for $A\beta_{42}$ fibrils	CSF	[188]
P_3/AgNPs SERS sensor	$A\beta_{42}$ human insulin	N9-(pyridin-2-ylmethyl)-N^6-methoxyadenine-functionalized P_3/AgNPs	76 aM for $A\beta_{42}$ 26 aM for human insulin	aCSF	[200]
AgNP/CS sensor AgNP/LID sensor	$ZnA\beta_{42}$ $CuA\beta_{42}$	–	1.5 nM for $ZnA\beta_{42}$ by AgNP/CS sensor 15 pM for $CuA\beta_{42}$ by AgNP/LID sensor	Plasma	[196]
Antibody					
AuNPs-coated ITO substrate	$A\beta_{40}$	β-amyloid antibody-modified Au-dot/ITO	100 fg/mL	–	[193]
$Fe_3O_4@SiO_2$ AuNPs	Tau	monoclonal anti-Tau-modified $Fe_3O_4@SiO_2$ DTNB-coded polyclonal anti-Tau-modified AuNPs	25 fM	–	[207]
AgNGS	$A\beta_{40}$ $A\beta_{42}$	$AgNGS_{[4\text{-}FBT]}$- $A\beta_{40}$ $AgNGS_{[4\text{-}BBT]}$- $A\beta_{42}$ CAb-MB	0.25 pg/mL for $A\beta_{40}$ 0.33 pg/mL for $A\beta_{42}$	Human serum	[206]
$Fe_3O_4@GOs$ Au@Ag probe	$A\beta_{42}M$ p-tau181	Anti-Aβ-amyloid antibody-modified $Fe_3O_4@GOs$ Anti-Aβ-amyloid antibody-modified Au@Ag probe Anti-Tau-amyloid antibody-modified $Fe_3O_4@GOs$ Anti-Tau-amyloid antibody-modified Au@Ag probe	1.62 fg/mL for $A\beta_{42}M$ 5.74 fg/mL for p-tau181	Serum	[194]
Au nanopillars AuNPs	Tau441	Half tau-antibody fragment-modified head-flocked Au nanopillars Half Cy3-conjugated tau polyclonal antibody-modified AuNPs	3.21 fM	Plasma	[195]
$Au@SiO_2$	$A\beta_{40}$ $A\beta_{42}$ Tau441 NfL	$A\beta_{40}/A\beta_{42}$/Tau/NfL monoclonal antibodies-modified nitrocellulose membrane $Au^{4-MBA}@SiO_2$ with $A\beta_{42}$/Tau monoclonal antibodies $Au^{DNTB}@SiO_2$ with $A\beta_{40}$/NfL monoclonal antibodies	191.2 fg/mL for $A\beta_{40}$ 138.1 fg/mL for $A\beta_{42}$ 257.1 fg/mL for Tau441 309.1 fg/mL for NfL	–	[210]
SIONs AuNPs	p-tau396, p-tau404	Antibody 3G5-SIONs 4-MBA@AuNP-HRP-R1	1.5 pg/mL	whole blood	[208]

(*continued on next page*)

Table 5. (continued)

Nanomaterials	Biomarkers	Recognition element	Limit of detection	Sample	References
Au-plasmonic shell attached polystyrene microsphere	$A\beta_{42}$ p-tau181	Aβ-Ab_1 NBA/AuNPs/Aβ-Ab_2 Tau-Ab_1 4-ATP/AuNPs/Tau-Ab_2	100 fg/mL	–	[211]
Aptamer					
AuNPs	AβO Tau381	4-AATP-coded PAapt-AuNPs DTNB-coded PAapt-AuNPs	37 pM for AβO 0.42 fM for Tau381	aCSF	[203]

Abbreviation: 4-AATP: 4-acetamidothiophenol, 4-ATP: 4-aminothiophenol, 4-BBT: 4-bromobenzenethiol, 4-FBT: 4-fluorobenzenethiol, 4-MBA: 4-mercaptobenzoic acid, Aβ-Ab: antibody-$A\beta_{42}$, AgNGS: Ag nanogap shell, $AgNGS_{[4\text{-BBT}]}$-$A\beta_{42}$: anti-$A\beta_{42}$ antibody-conjugated AgNGS entrapping 4-BBT, $AgNGS_{[4\text{-FBT}]}$-$A\beta_{40}$: anti-$A\beta_{40}$ antibody-conjugated AgNGS entrapping 4-FBT, Au@Ag probe: gold-silver alloy nanoprobe, AuNPs: gold nanoparticles, CAb-MB: capture Ab-conjugated magnetic bead, Chiral Pt@Au TNRs: chiral triangular Au nanorings fabricated with a platinum framework, CS: chitosan, $CuA\beta_{42}$: Cu^{2+} assisted aggregated $A\beta_{42}$, DTNB: 5,5′-dithio-bis (2-nitrobenzoic acid), Fe_3O_4@GOs: magnetic graphene oxide, HRP: horseradish peroxidase, ITO: indium tin oxide, LID: laser induced deposition, NBA: Nile rule A, NfL: neurofilament light chain protein, P_3: ligand (100 mg)-impregnated polyacrylonitrile nanofibers mat, PAapt-AuNPs: polyA aptamer−AuNPs conjugates, RB: rose bengal, SION: superparamagnetic iron oxide nanoparticles, Tau-Ab: antibody-Tau, $ZnA\beta_{42}$: Zn^{2+} assisted aggregated $A\beta_{42}$.

nanomaterials in the development of SERS-based sensors [193,201−203], so as to refine the selectivity, avoiding false quantification of targets due to the interference of analogs. SERS tags (dye)-coded nanomaterials coupled with aptamers or antibodies as the recognition element greatly enhance the Raman intensity relied on these molecules with intrinsically strong Raman signals. Take aptamer-based strategy, for example, Zhang et al. developed an aptamer-based SERS sensing platform by designing two Raman dye-coded AuNPs conjugates for a multiplexed detection of $A\beta_{42}$ oligomers and Tau proteins. In this study, the aptamer sequences were extended with poly consecutive adenine (polyA) sequences (PApt), which can anchor onto the surface of AuNPs by high affinity without modification and prevent adjacent AuNPs from aggregation [204]. In the presence of targets, PApt can bind with corresponding targets and detach from AuNPs. Subsequently, AuNPs will aggregate by the plasmonic coupling effect, and a distinct SERS signal can exhibit due to the enhancement of the electrostatic field from hot spots [203]. Yang et al. have developed sandwich antibody-based SERS sensors for detecting Tau441. This design aims to position Tau441 close to the hot spot during antigen−antibody interaction. The half antibody fragment is placed on the head-flocked gold nanopillar substrate, while the Cy3-half antibody fragment is attached to AuNPs, serving as SERS nanotags [195]. The researchers reduced the size of antibodies by treating tris(2-carboxyethyl) phosphine (TCEP) to break apart the disulfide bonds and divide the antibody into two fragments. This process resulted in half antibody fragments that could be placed close to hot spots on the adjacent point between gold nanopillars on the substrate [205]. The electromagnetic field greatly enhanced and generated a higher Raman signal after the interaction of analytes and antibodies adjacent to hot spots. The sensor achieved a 135-fold increase in sensitivity compared to the antibody-based sensor. Yang et al. constructed two SERS signal probes of $A\beta_{40}$ and $A\beta_{42}$ antibodies-conjugated Ag nanogap shells (AgNGS), which respectively entrapped with Raman dyes, namely 4-fluorobenzenethiol (4-FBT) and 4-bromobenzenethiol (4-BBT), inside gaps of AgNPs synthesized on the surface of thio-functionalized SiNPs. A SERS-based sandwich immunosensor was developed for multiplex detection of AD biomarkers by the antibody-conjugated AgNGS entrapping Raman dyes and captured antibody-conjugated magnetic bead which can recognize the 1−16 sequence of $A\beta_{40}$ and $A\beta_{42}$. Attributed to different Raman signals exhibited from the 4-FBT

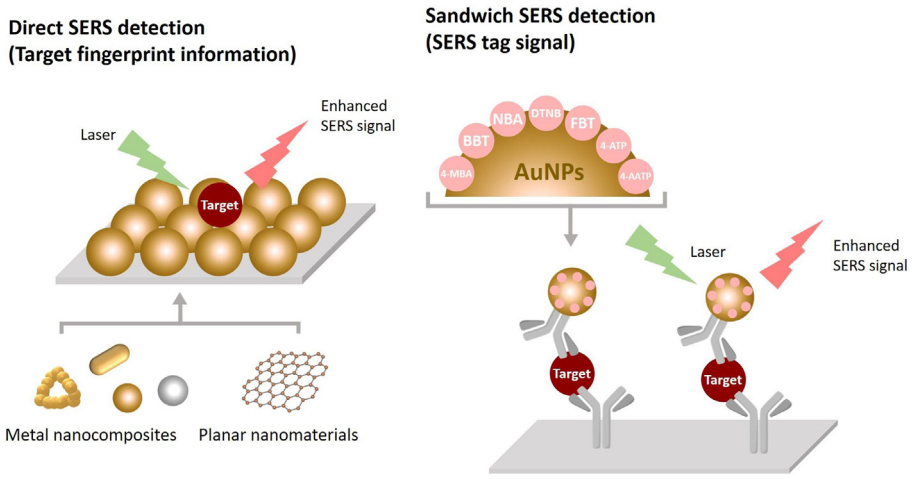

Fig. 5. SERS strategies for AD biomarkers based on nanomaterials with different mechanisms.

and the 4-BBT, the simultaneous detection of $A\beta_{40}$ and $A\beta_{42}$ can be achieved, and enhanced Raman intensity was acquired to be 10^7 for the limit of detection for amounts as low as 0.25 pg/mL [206].

Other studies have also used sandwich immunoassay detection strategies with different platforms to detect AD biomarkers. Zengin et al. constructed a SERS-based sandwich immunoassay for the detection of Tau coupled with a magnetic separation technique by 5,5′-dithio bis-(2-nitrobenzoic acid) (DNTB)-coded AuNPs modified with antibody and antibody-functionalized magnetic silica particles (Fe_3O_4@SiO_2) [207]. Zhang et al. established a magnetic dual-mode immunosensor for the detection of p-tau396 and p-tau404 in whole blood samples. They designed a signal antibody composed of HRP-labeled antibody-functionalized and 4-mercaptobenzoic acid (4-MBA) capped AuNPs (4-MBA@AuNPs-HRP-R1 probe), which can be simultaneously detected targets in Raman and colorimetric modes. This immunosensor can detect p-tau396 and p-tau404 in blood with as low as 1.5 pg/mL in SERS mode and 24 pg/mL in colorimetric mode [208]. Yu et al. fabricated an immunoassay on a magnetic graphene oxide (Fe_3O_4@GO) substrate for the detection of $A\beta_{42}$ and p-tau181 with the antibody-functionalized and 4-MBA coded tannin-capped AgNPs as a Raman enhanced signal probe [209]; Zhan et al. constructed an immunolateral flow assay, using Au@SiO_2 coded with 4-MBA and DNTB as SERS nanotags, for accomplishing the simultaneous detection of $A\beta_{40}$, $A\beta_{42}$, Tau, and NfL with two test lines [210]; Sun et al. established an immune-sensor in a microfluidic chip for the dual detection of Aβ and Tau with Nile rule A and 4-aminothiophenol-coded AuNPs as signal indicators, respectively [211].

According to the clinical research relevant to AD biomarkers, diagnostic values of these substances range from nano to pico orders of magnitude [24,25]. This review introduced many SERS-based sensors for the detection of AD biomarkers, some of which possess very high sensitivity and even reach femto or atto orders of magnitude. To obtain a higher sensitivity, it is crucial to find out the hot spot of nanomaterials against targets. It is also very important to manipulate the location of targets that interact with the SERS system. However, most researchers used antibodies to enhance the selectivity of SERS-based sensors. Antibodies possess a rigid and big-sized structure, which may limit the performance of SERS due to the large distance between SERS signal indicator (target or nanotag) and SERS-induced substrate (nanomaterials). To improve this drawback, half antibody-fragment was utilized to reduce the distance [195]. However, few studies used aptamer in such a scenario. In addition to specifically binding with targets, aptamer also provided properties of stability and ease of modification. Thus, the smaller size of aptamer exhibits less steric hindrance compared with antibodies [212]. The flexible structure of the aptamer may facilitate the manipulation of targets that reach the hot spot. Therefore, the aptamer technique may also be an ideal candidate for developing SERS-based sensors.

4. Conclusion

In the timeline of diagnosing AD biomarkers before 2014, most of the methods for detecting AD biomarkers were strategized in a CSF sample. Although the strategy of detecting AD biomarkers in a blood-based sample was also carried out in some studies, those outcomes showed no apparent

evidence to demonstrate AD biomarkers in blood-based samples associated with the pathogenesis of AD [213]. There are several challenges associated with detecting AD biomarkers in blood-based samples. For example, levels of biomarkers in blood-based samples were lower than those in CSF samples due to the blood–brain barrier, which limits the influx of AD biomarkers into the blood circulatory system; proteolytic degradation or nonspecific interaction AD biomarkers with protein interferences in blood-based samples also influence the accurate quantification, especially for the antibody-based methods due to the hindrance of binding sites against targets [214]. However, even if confronted with many challenges during the research, the investigation of AD biomarkers in blood-based samples was still continuously implemented, which is attributed to the major drawback of collecting CSF samples. The collection of a CSF sample is performed by a lumbar puncture, which is an invasive treatment that patients are reluctant to undergo. Besides, such a sample collection method also discourages researchers from promoting the strategy of the early diagnosis of AD. Compared to the intrusive sample collection of CSF samples, the blood test is still an appealing and expected way to diagnose AD [215]. Notably, from 2014 to 2022, research on AD biomarkers in blood-based samples dramatically progressed due to sophisticated analytical techniques with high sensitivity, allowing researchers to effectively distinguish the different levels of AD biomarkers between healthy individuals and AD patients. In addition, it was crucial to establish standardized guidelines for collecting and storing blood-based samples to ensure accurate research outcomes [216]. According to the preanalytic processing guideline established by O'Bryant and co-workers [217], they summarized cohorts undergoing the clinical detection of AD biomarkers in blood-based samples from the collection of blood samples to the storage of plasma or serum samples. Briefly, the storage temperature of plasma samples is the most important point that prevents samples from enzymatic activity to diminish the influence of the proteolytic degradation of the protein. The long-term storage of plasma samples should be at −80 °C or in liquid nitrogen. In addition to the sample collection and storage, the selection of subjects with various conditions should also consider demographic characteristics, genomic type of *ApoE*, non-AD comorbidities, diet, medications, and so on. These variables can also affect the detection outcome and should be appropriately incorporated into the statistical analysis.

For the development of analytical techniques for the detection of AD biomarkers in blood-based samples, optical biosensing techniques possess great potential to detect AD biomarkers, which were discussed in this review. Nanomaterials have extremely small sizes, high specific surface areas, and unique optical properties. Therefore, combining them with optical sensors can amplify the detection signal and improve the sensitivity. It also has the advantage of improving its selectivity, stability, and system reproducibility. In nanomaterials-based optical sensors, the colorimetric method for detecting biomarkers has the advantages of easy operation and naked-eye observation. However, its sensitivity is only nM, making it challenging to apply to the detection of biomarkers in the body. In the future, combining with isothermal signal amplification technology to improve sensitivity will be a potential strategy to be developed into a point-of-care testing reagent. The systems of SPR and LSPR possess relatively high sensitivity, which can reach a femto or atto-scale in the detection of protein or microRNA, respectively. The LSPR-based technique provided an outstanding ability with a very high sensitivity for genotype detection. The detection limit for AD biomarkers can reach the pico-scale level in fluorometry. However, the most common sample treatment method for biomarker detection involves dilution. Therefore, employing isothermal signal amplification techniques based on nucleic acid branch migration in combination with nanomaterial-based fluorometry can enhance sensitivity, particularly when utilizing an aptamer-based approach. For SERS-based technique, a higher sensitivity can also be obtained down to the level of femto and atto-scale. However, the detection signal of SERS is acquired from the molecular vibration of the target. It is inevitable to obtain other signals from the background, especially when detecting targets in a complex matrix. Therefore, using antibodies and aptamers is an effective way to improve the selectivity and reduce the interference from sample matrices.

Based on the stability, reproducibility and unique optical properties of fabricated nanomaterials, their integration into optical sensors significantly enhances detection performance, particularly for low-concentration AD biomarkers in pico to femto scales. On the other hand, multiple assessments of AD biomarkers can better reflect the correlation between biomarkers and AD progression than relying on a single biomarker. As a result, the development of a multiplex biomarker detection platform can also broaden the utilization of analytical technology in clinical research and testing.

Conflict of interest

The authors have declared no conflict of interest.

References

[1] Association As. 2021 Alzheimer's disease facts and figure. 2021.
[2] Gella A, Durany N. Oxidative stress in Alzheimer disease. Cell Adh Migr 2009;3:88–93.
[3] Akiyama H, Arai T, Kondo H, Tanno E, Haga C, Ikeda K. Cell mediators of inflammation in the Alzheimer disease brain. Alzheimer Dis Assoc Disord 2000;14:S47–53.
[4] Braak H, Braak E, Bohl J. Staging of Alzheimer-related cortical destruction. Eur Neurol 1993;33:403–8.
[5] Guerchet M, Prince M, Prina M. An update to the estimates in the World Alzheimer Report 2015: Numbers of people with dementia worldwide. London, UK: Alzheimer's Disease International; 2020.
[6] Gauthier SR-NP, Morais JA, Webster C. World Alzheimer report 2021: journey through the diagnosis of dementia. London, UK: Alzheimer's Disease International; 2021.
[7] FDA. FDA converts novel Alzheimer's disease treatment to traditional approval: action follows confirmatory trial to verify clinical benefit. FDA; 2023. Available at: https://www.fda.gov/news-events/press-announcements/fda-converts-novel-alzheimers-disease-treatment-traditional-approval. [Accessed 1 March 2024].
[8] Jack CR, Bennett DA, Blennow K, Carrillo MC, Dunn B, Haeberlein SB, et al. NIA-AA research framework: toward a biological definition of Alzheimer's disease. Alzheimers Dement 2018;14:535–62.
[9] Tao QQ, Lin RR, Wu ZY. Early diagnosis of Alzheimer's disease: moving toward a blood-based biomarkers era. Clin Interv Aging 2023;18:353–8.
[10] Zetterberg H, Schott JM. Biomarkers for Alzheimer's disease beyond amyloid and tau. Nat Med 2019;25:201–3.
[11] Hansson O. Biomarkers for neurodegenerative diseases. Nat Med 2021;27:954–63.
[12] Rani S, Dhar SB, Khajuria A, Gupta D, Jaiswal PK, Singla N, et al. Advanced overview of biomarkers and techniques for early diagnosis of Alzheimer's disease. Cell Mol Neurobiol 2023;43:2491–523.
[13] Palmqvist S, Tideman P, Cullen N, Zetterberg H, Blennow K, Dage JL, et al. Prediction of future Alzheimer's disease dementia using plasma phospho-tau combined with other accessible measures. Nat Med 2021;27:1034–42.
[14] Hawksworth J, Fernandez E, Gevaert K. A new generation of AD biomarkers: 2019 to 2021. Ageing Res Rev 2022;79:101654.
[15] Zheng H, Koo EH. The amyloid precursor protein: beyond amyloid. Mol Neurodegener 2006;1:5.
[16] Thinakaran G, Koo EH. Amyloid precursor protein trafficking, processing, and function. J Biol Chem 2008;283:29615–9.
[17] Murphy MP, LeVine 3rd H. Alzheimer's disease and the amyloid-beta peptide. J Alzheimers Dis 2010;19:311–23.
[18] Querfurth HW, LaFerla FM. Alzheimer's disease. N Engl J Med 2010;362:329–44.
[19] Willbold D, Strodel B, Schröder GF, Hoyer W, Heise H. Amyloid-type protein aggregation and prion-like properties of amyloids. Chem Rev 2021;121:8285–307.
[20] Madhu P, Mukhopadhyay S. Distinct types of amyloid-β oligomers displaying diverse neurotoxicity mechanisms in Alzheimer's disease. J Cell Biochem 2021;122:1594–608.
[21] Hansson O, Edelmayer RM, Boxer AL, Carrillo MC, Mielke MM, Rabinovici GD, et al. The Alzheimer's Association appropriate use recommendations for blood biomarkers in Alzheimer's disease. Alzheimers Dement 2022;18:2669–86.
[22] Mulder C, Verwey NA, van der Flier WM, Bouwman FH, Kok A, van Elk EJ, et al. Amyloid-β(1-42), total tau, and phosphorylated tau as cerebrospinal fluid biomarkers for the diagnosis of Alzheimer disease. Clin Chem 2010;56:248–53.
[23] Hansson O, Zetterberg H, Buchhave P, Andreasson U, Londos E, Minthon L, et al. Prediction of Alzheimer's disease using the CSF Aβ42/Aβ40 ratio in patients with mild cognitive impairment. Dement Geriatr Cogn 2007;23:316–20.
[24] Chiu MJ, Chen TF, Hu CJ, Yan SH, Sun Y, Liu BH, et al. Nanoparticle-based immunomagnetic assay of plasma biomarkers for differentiating dementia and prodromal states of Alzheimer's disease - a cross-validation study. Nanomedicine 2020;28:102182.
[25] Youn YC, Lee BS, Kim GJ, Ryu JS, Lim K, Lee R, et al. Blood amyloid-β oligomerization as a biomarker of Alzheimer's disease: a blinded validation study. J Alzheimers Dis 2020;75:493–9.
[26] Savage MJ, Kalinina J, Wolfe A, Tugusheva K, Korn R, Cash-Mason T, et al. A sensitive Aβ oligomer assay discriminates Alzheimer's and aged control cerebrospinal fluid. J Neurosci 2014;34:2884–97.
[27] Sergeant N, Delacourte A, Buée L. Tau protein as a differential biomarker of tauopathies. Biochim Biophys Acta, Mol Basis Dis 2005;1739:179–97.
[28] Laske C, Stransky E, Fritsche A, Eschweiler G, Leyhe T. Inverse association of cortisol serum levels with T-tau, P-tau181 and P-tau 231 peptide levels and T-tau/Aβ 1-42 ratios in CSF in patients with mild Alzheimer's disease dementia. Eur Arch Psychiatr Clin Neurosci 2009;259:80–5.
[29] Martin L, Latypova X, Terro F. Post-translational modifications of tau protein: implications for Alzheimer's disease. Neurochem Int 2011;58:458–71.
[30] Brunello CA, Merezhko M, Uronen RL, Huttunen HJ. Mechanisms of secretion and spreading of pathological tau protein. Cell Mol Life Sci 2020;77:1721–44.
[31] Chan HN, Xu D, Ho SL, He D, Wong MS, Li HW. Highly sensitive quantification of Alzheimer's disease biomarkers by aptamer-assisted amplification. Theranostics 2019;9:2939–49.
[32] Janelidze S, Stomrud E, Smith R, Palmqvist S, Mattsson N, Airey DC, et al. Cerebrospinal fluid p-tau217 performs better than p-tau181 as a biomarker of Alzheimer's disease. Nat Commun 2020;11:1683.
[33] Milà-Alomà M, Ashton NJ, Shekari M, Salvadó G, Ortiz-Romero P, Montoliu-Gaya L, et al. Plasma p-tau231 and p-tau217 as state markers of amyloid-β pathology in preclinical Alzheimer's disease. Nat Med 2022;28:1797–801.
[34] Mendes AJ, Ribaldi F, Lathuiliere A, Ashton NJ, Janelidze S, Zetterberg H, et al. Head-to-head study of diagnostic accuracy of plasma and cerebrospinal fluid p-tau217 versus p-tau181 and p-tau231 in a memory clinic cohort. J Neurol 2024;271:2053–66.
[35] Forlenza OV, Radanovic M, Talib LL, Aprahamian I, Diniz BS, Zetterberg H, et al. Cerebrospinal fluid biomarkers in Alzheimer's disease: diagnostic accuracy and prediction of dementia. Alzheimers Dement 2015;1:455–63.
[36] Gaetani L, Parnetti L, Calabresi P, Di Filippo M. Tracing neurological diseases in the presymptomatic phase: insights from neurofilament light chain. Front Neurosci-Switz 2021;15:672954.
[37] Preische O, Schultz SA, Apel A, Kuhle J, Kaeser SA, Barro C, et al. Serum neurofilament dynamics predicts neurodegeneration and clinical progression in presymptomatic Alzheimer's disease. Nat Med 2019;25:277–83.
[38] Jung YJ, Damoiseaux JS. The potential of blood neurofilament light as a marker of neurodegeneration for Alzheimer's disease. Brain 2024;147:12–25.
[39] Teunissen CE, Verberk IMW, Thijssen EH, Vermunt L, Hansson O, Zetterberg H, et al. Blood-based biomarkers for Alzheimer's disease: towards clinical implementation. Lancet Neurol 2022;21:66–77.
[40] Lewczuk P, Ermann N, Andreasson U, Schultheis C, Podhorna J, Spitzer P, et al. Plasma neurofilament light as a

potential biomarker of neurodegeneration in Alzheimer's disease. Alzheimer's Res Ther 2018;10:71.
[41] Weston PSJ, Poole T, O'Connor A, Heslegrave A, Ryan NS, Liang YY, et al. Longitudinal measurement of serum neurofilament light in presymptomatic familial Alzheimer's disease. Alzheimer's Res Ther 2019;11:19.
[42] Benedet AL, Leuzy A, Pascoal TA, Ashton NJ, Mathotaarachchi S, Savard M, et al. Stage-specific links between plasma neurofilament light and imaging biomarkers of Alzheimer's disease. Brain 2020;143:3793−804.
[43] Budelier MM, He Y, Barthelemy NR, Jiang H, Li Y, Park E, et al. A map of neurofilament light chain species in brain and cerebrospinal fluid and alterations in Alzheimer's disease. Brain Commun 2022;4:fcac045.
[44] Xiang Y, Xin JY, Le WD, Yang YJ. Neurogranin: a potential biomarker of neurological and mental diseases. Front Aging Neurosci 2020;12:584743.
[45] Saunders T, Gunn C, Blennow K, Kvartsberg H, Zetterberg H, Shenkin SD, et al. Neurogranin in Alzheimer's disease and ageing: a human post-mortem study. Neurobiol Dis 2023;177:105991.
[46] Tarawneh R, D'Angelo G, Crimmins D, Herries E, Griest T, Fagan AM, et al. Diagnostic and prognostic utility of the synaptic marker neurogranin in Alzheimer disease. JAMA Neurol 2016;73:561−71.
[47] Wellington H, Paterson RW, Portelius E, Törnqvist U, Magdalinou N, Fox NC, et al. Increased CSF neurogranin concentration is specific to Alzheimer disease. Neurology 2016;86:829−35.
[48] Willemse EAJ, Sieben A, Somers C, Vermeiren Y, De Roeck N, Timmers M, et al. Neurogranin as biomarker in CSF is non-specific to Alzheimer's disease dementia. Neurobiol Aging 2021;108:99−109.
[49] Sharma M, Burré J. α-Synuclein in synaptic function and dysfunction. Trends Neurosci 2023;46:153−66.
[50] Carnazza KE, Komer LE, Xie YX, Pineda A, Briano JA, Gao V, et al. Synaptic vesicle binding of α-synuclein is modulated by β- and γ-synucleins. Cell Rep 2022;39.
[51] Bousiges O, Philippi N, Lavaux T, Perret-Liaudet A, Lachmann I, Schaeffer-Agalède C, et al. Differential diagnostic value of total alpha-synuclein assay in the cerebrospinal fluid between Alzheimer's disease and dementia with Lewy bodies from the prodromal stage. Alzheimer's Res Ther 2020;12:120.
[52] Shi M, Tang L, Toledo JB, Ginghina C, Wang H, Aro P, et al. Cerebrospinal fluid α-synuclein contributes to the differential diagnosis of Alzheimer's disease. Alzheimers Dement 2018;14:1052−62.
[53] Shim KH, Kang MJ, Suh JW, Pyun JM, Ryoo N, Park YH, et al. CSF total tau/α-synuclein ratio improved the diagnostic performance for Alzheimer's disease as an indicator of tau phosphorylation. Alzheimer's Res Ther 2020;12:83.
[54] Majbour NK, Chiasserini D, Vaikath NN, Eusebi P, Tokuda T, van de Berg W, et al. Increased levels of CSF total but not oligomeric or phosphorylated forms of alpha-synuclein in patients diagnosed with probable Alzheimer's disease. Sci Rep 2017;7:40263.
[55] Oeckl P, Metzger F, Nagl M, von Arnim CAF, Halbgebauer S, Steinacker P, et al. Alpha-, beta-, and gamma-synuclein quantification in cerebrospinal fluid by multiple reaction monitoring reveals increased concentrations in Alzheimer's and Creutzfeldt-Jakob disease but no alteration in synucleinopathies. Mol Cell Proteomics 2016;15:3126−38.
[56] Garland EF, Hartnell IJ, Boche D. Microglia and astrocyte Function and communication: what do we know in humans? Front Neurosci 2022;16:824888.
[57] Singh D. Astrocytic and microglial cells as the modulators of neuroinflammation in Alzheimer's disease. J Neuroinflammation 2022;19:206.
[58] Knapskog AB, Henjum K, Idland AV, Eldholm RS, Persson K, Saltvedt I, et al. Cerebrospinal fluid sTREM2 in Alzheimer's disease: comparisons between clinical presentation and AT classification. Sci Rep-Uk 2020;10:15886.
[59] Morenas-Rodríguez E, Li Y, Nuscher B, Franzmeier N, Xiong CJ, Suárez-Calvet M, et al. Soluble TREM2 in CSF and its association with other biomarkers and cognition in autosomal-dominant Alzheimer's disease: a longitudinal observational study. Lancet Neurol 2022;21:329−41.
[60] Ma LZ, Tan L, Bi YL, Shen XN, Xu W, Ma YH, et al. Dynamic changes of CSF sTREM2 in preclinical Alzheimer's disease: the CABLE study. Mol Neurodegener 2020;15:25.
[61] Suárez-Calvet M, Morenas-Rodríguez E, Kleinberger G, Schlepckow K, Caballero MAA, Franzmeier N, et al. Early increase of CSF sTREM2 in Alzheimer's disease is associated with tau related-neurodegeneration but not with amyloid- pathology. Mol Neurodegener 2019;14:1.
[62] Schlepckow K, Morenas-Rodríguez E, Hong S, Haass C. Stimulation of TREM2 with agonistic antibodies-an emerging therapeutic option for Alzheimer's disease. Lancet Neurol 2023;22:1048−60.
[63] Yang XY, Wen J, Yang H, Jones IR, Zhu XD, Liu WF, et al. Functional characterization of Alzheimer's disease genetic variants in microglia. Nat Genet 2023:1735−44.
[64] Bekris LM, Khrestian M, Dyne E, Shao Y, Pillai JA, Rao SM, et al. Soluble TREM2 and biomarkers of central and peripheral inflammation in neurodegenerative disease. J Neuroimmunol 2018;319:19−27.
[65] Kim B, Suh E, Nguyen AT, Prokop S, Mikytuck B, Olatunji OA, et al. TREM2 risk variants are associated with atypical Alzheimer's disease. Acta Neuropathol 2022;144:1085−102.
[66] Deming Y, Filipello F, Cignarella F, Cantoni C, Hsu S, Mikesell R, et al. The MS4A gene cluster is a key modulator of soluble TREM2 and Alzheimer's disease risk. Sci Transl Med 2019;11:eaau2291.
[67] Carter SF, Herholz K, Rosa-Neto P, Pellerin L, Nordberg A, Zimmer ER. Astrocyte biomarkers in Alzheimer's disease. Trends Mol Med 2019;25:77−95.
[68] Pelkmans W, Shekari M, Brugulat-Serrat A, Sánchez-Benavides G, Minguillón C, Fauria K, et al. Astrocyte biomarkers GFAP and YKL-40 mediate early Alzheimer's disease progression. Alzheimers Dement 2023:483−93.
[69] Yang ZS, Sreenivasan K, Strom ENT, Osse AML, Pasia LG, Cosme CG, et al. Clinical and biological relevance of glial fibrillary acidic protein in Alzheimer's disease. Alzheimer's Res Ther 2023;15:190.
[70] Chatterjee P, Pedrini S, Doecke JD, Thota R, Villemagne VL, Doré V, et al. Plasma Aβ42/40 ratio, p-tau181, GFAP, and NfL across the Alzheimer's disease continuum: a cross-sectional and longitudinal study in the AIBL cohort. Alzheimers Dement 2023;19:1117−34.
[71] Stevenson-Hoare J, Heslegrave A, Leonenko G, Fathalla D, Bellou E, Luckcuck L, et al. Plasma biomarkers and genetics in the diagnosis and prediction of Alzheimer's disease. Brain 2023;146:690−9.
[72] Zhao T, Su ZP, Li YC, Zhang XR, You Q. Chitinase-3 like-protein-1 function and its role in diseases. Signal Transduct Tar 2020;5.
[73] Prins S, de Kam ML, Teunissen CE, Groeneveld GJ. Inflammatory plasma biomarkers in subjects with preclinical Alzheimer's disease. Alzheimer's Res Ther 2022;14:106.
[74] Meneses A, Koga S, O'Leary J, Dickson DW, Bu GJ, Zhao N. TDP-43 pathology in Alzheimer's disease. Mol Neurodegener 2021;16:84.
[75] Prater KE, Latimer CS, Jayadev S. Glial TDP-43 and TDP-43 induced glial pathology, focus on neurodegenerative proteinopathy syndromes. Glia 2022;70:239−55.
[76] Bellenguez C, Küçükali F, Jansen IE, Kleineidam L, Moreno-Grau S, Amin N, et al. New insights into the genetic etiology of Alzheimer's disease and related dementias. Nat Genet 2022;54:412−36.
[77] Cruchaga C, Chakraverty S, Mayo K, Vallania FLM, Mitra RD, Faber K, et al. Rare variants in APP, PSEN1 and

PSEN2 increase risk for AD in late-onset Alzheimer's disease families. PLoS One 2012;7:e31039.
[78] Reitz C, Pericak-Vance MA, Foroud T, Mayeux R. A global view of the genetic basis of Alzheimer disease. Nat Rev Neurol 2023;19:261−77.
[79] Corder EH, Saunders AM, Strittmatter WJ, Schmechel DE, Gaskell PC, Small GW, et al. Gene dose of apolipoprotein E type 4 allele and the risk of Alzheimer's disease in late onset families. Science 1993;261:921−3.
[80] Rajabli F, Beecham GW, Hendrie HC, Baiyewu O, Ogunniyi A, Gao S, et al. A locus at 19q13.31 significantly reduces the ε4 risk for Alzheimer's Disease in African Ancestry. PLoS Genet 2022;18:e1009977.
[81] Müller M, Kuiperij HB, Claassen JA, Küsters B, Verbeek MM. MicroRNAs in Alzheimer's disease: differential expression in hippocampus and cell-free cerebrospinal fluid. Neurobiol Aging 2014;35:152−8.
[82] Lusardi TA, Phillips JI, Wiedrick JT, Harrington CA, Lind B, Lapidus JA, et al. MicroRNAs in human cerebrospinalfluid as biomarkers for Alzheimer's disease. J Alzheimers Dis 2017;55:1223−33.
[83] van den Berg MMJ, Krauskopf J, Ramaekers JG, Kleinjans JCS, Prickaerts J, Briedé JJ. Circulating microRNAs as potential biomarkers for psychiatric and neurodegenerative disorders. Prog Neurobiol 2020;185:101732.
[84] Swarbrick S, Wragg N, Ghosh S, Stolzing A. Systematic review of miRNA as biomarkers in Alzheimer's disease. Mol Neurobiol 2019;56:6156−67.
[85] Villa C, Ridolfi E, Fenoglio C, Ghezzi L, Vimercati R, Clerici F, et al. Expression of the transcription factor and its regulatory hsa-miR-29b in peripheral blood mononuclear cells from patients with Alzheimer's cisease. J Alzheimers Dis 2013;35:487−94.
[86] Rani S, Dhar SB, Khajuria A, Gupta D, Jaiswal PK, Singla N, et al. Advanced overview of biomarkers and techniques for early diagnosis of Alzheimer's disease. Cell Mol Neurobiol 2023;43:2491−523.
[87] Banzhaf-Strathmann J, Benito E, May S, Arzberger T, Tahirovic S, Kretzschmar H, et al. MicroRNA-125b induces tau hyperphosphorylation and cognitive deficits in Alzheimer's disease. EMBO J 2014;33:1667−80.
[88] Tan L, Yu JT, Liu QY, Tan MS, Zhang W, Hu N, et al. Circulating miR-125b as a biomarker of Alzheimer's disease. J Neurol Sci 2014;336:52−6.
[89] Kim DM, Yoo SM. Colorimetric systems for the detection of bacterial contamination: strategy and applications. Biosensors 2022;12:532.
[90] Ong JJ, Pollard TD, Goyanes A, Gaisford S, Elbadawi M, Basit AW. Optical biosensors - illuminating the path to personalized drug dosing. Biosens Bioelectron 2021;188:113331.
[91] Cui YY, Zhao J, Li HD. Chromogenic mechanisms of colorimetric sensors based on gold nanoparticles. Sensors 2023;13:801.
[92] Damborský P, Švitel J, Katrlík J. Optical biosensors. Essays Biochem 2016;60:91−100.
[93] Khachornsakkul K, Tiangtrong A, Suwannasom A, Sangkharoek W, Jamjumrus O, Dungchai W. Distance-based β-amyloid protein detection on PADs for the scanning and subsequent follow-up of Alzheimer's disease in human urine samples. Analyst 2022;147:695−703.
[94] Ito S, Yamamoto D. Mechanism for the color change in bromocresol purple bound to human serum albumin. Clin Chim Acta 2010;411:294−5.
[95] Chen GY, Chai TQ, Wang JL, Yang FQ. Recent advances in the colorimetric and fluorescence analysis of bioactive small-molecule compounds based on the enzyme-like activity of nanomaterials. J Pharmaceut Biomed 2023;236:115695.
[96] Josephy PD, Eling T, Mason RP. The horseradish peroxidase-catalyzed oxidation of 3,5,3',5'-tetramethylbenzidine - free-radical and charge-transfer complex intermediates. J Biol Chem 1982;257:3669−75.
[97] Duan CJ, Jiao J, Zheng J, Li DY, Ning LM, Xiang Y, et al. Polyvalent biotinylated aptamer scaffold for rapid and sensitive detection of Tau proteins. Anal Chem 2020;92:15162−8.
[98] Chen M, Man YZ, Xu SL, Wu HJ, Ling PH, Gao F. A label-free dually-amplified aptamer sensor for the specific detection of amyloid-beta peptide oligomers in cerebrospinal fluids. Anal Chim Acta 2023;1266:341298.
[99] Khan ZA, Park S. AuNPs-Aβ-Ni-HRP sandwich assay: a new sensitive colorimetric method for the detection of Aβ (1-40). Talanta 2022;237:122946.
[100] Wang XY, Hu YH, Wei H. Nanozymes in bionanotechnology: from sensing to therapeutics and beyond. Inorg Chem Front 2016;3:41−60.
[101] Yang B, Li JP, Deng H, Zhang LM. Progress of mimetic enzymes and their applications in chemical sensors. Crit Rev Anal Chem 2016;46:469−81.
[102] Zhou X, Wang SL, Zhang C, Lin YL, Lv J, Hu SY, et al. Colorimetric determination of amyloid-β peptide using MOF-derived nanozyme based on porous ZnO-Co_3O_4 nanocages. Microchim Acta 2021;188:56.
[103] Lu KD, Aung T, Guo NN, Weichselbaum R, Lin WB. Nanoscale metal-organic frameworks for therapeutic, imaging, and sensing applications. Adv Mater 2018;30:1707634.
[104] Hu S, Yang CW, Li YQ, Luo QM, Luo HM. Nanozyme sensor array based on manganese dioxide for the distinction between multiple amyloid β peptides and their dynamic aggregation process. Biosens Bioelectron 2022;199:113881.
[105] Naresh V, Lee N. A review on biosensors and recent development of nanostructured materials-enabled biosensors. Sensors 2021;21:1109.
[106] Link S, El-Sayed MA. Size and temperature dependence of the plasmon absorption of colloidal gold nanoparticles. J Phys Chem B 1999;103:4212−7.
[107] Zhu X, Zhang NN, Zhang YT, Liu BX, Chang Z, Zhou YL, et al. A sensitive gold nanoparticle-based aptasensor for colorimetric detection of Aβ-40 oligomers. Anal Methods 2018;10:641−5.
[108] Tu Y, Wu JJ, Chai KK, Hu XC, Hu Y, Shi S, et al. A turn-on unlabeled colorimetric biosensor based on aptamer-AuNPs conjugates for amyloid- β oligomer detection. Talanta 2023;260:124649.
[109] Ghasemi F, Hormozi-Nezhad MR, Mahmoudi M. Label-free detection of β-amyloid peptides (Aβ40 and Aβ42): a colorimetric sensor array for plasma monitoring of Alzheimer's disease. Nanoscale 2018;10:6361−8.
[110] Mikkonen S, Jacksén J, Roeraade J, Thormann W, Emmer A. Microfluidic isoelectric focusing of amyloid beta peptides followed by micropillar-matrix-assisted laser desorption ionization-mass spectrometry. Anal Chem 2016;88:10044−51.
[111] Liu C, You X, Lu D, Shi G, Deng J, Zhou T. Gelsolin encountering Ag nanorods/triangles: an aggregation-based colorimetric sensor array for in vivo monitoring the cerebrospinal Aβ42% as an indicator of Cd^{2+} exposure-related Alzheimer's disease pathogenesis. ACS Appl Bio Mater 2020;3:7965−73.
[112] Nair RV, Yi PJ, Padmanabhan P, Gulyás B, Murukeshan VM. Au nano-urchins enabled localized surface plasmon resonance sensing of beta amyloid fibrillation. Nanoscale Adv 2020;2:2693−8.
[113] Kim H, Lee JU, Song S, Kim S, Sim SJ. A shape-code nanoplasmonic biosensor for multiplex detection of Alzheimer's disease biomarkers. Biosens Bioelectron 2018;101:96−102.
[114] Song S, Lee JU, Jeon MJ, Kim S, Sim SJ. Detection of multiplex exosomal miRNAs for clinically accurate diagnosis of Alzheimer's disease using label-free plasmonic biosensor based on DNA-assembled advanced plasmonic architecture. Biosens Bioelectron 2022;199:113864.
[115] Wu WT, Chen CH, Chiang CY, Chau LK. Effect of surface coverage of gold nanoparticles on the refractive index

sensitivity in fiber-optic nanoplasmonic sensing. Sensors 2018;18:1759.
[116] Chang JH, Wang CH, Chang TC, Wen WC, Huang CJ, Chen YL, et al. Apolipoprotein E genetic analysis in unamplified genomic DNA extracts by ligase reaction and fiber optic particle plasmon resonance biosensor. Sensor Actuator B Chem 2023;393:134237.
[117] Neuman KC, Nagy A. Single-molecule force spectroscopy: optical tweezers, magnetic tweezers and atomic force microscopy. Nat Methods 2008;5:491−505.
[118] Zheng Y, Geng XH, Yang XH, Li SY, Liu YQ, Liu XF, et al. Exploring interactions of aptamers with Aβ40 amyloid aggregates and its application: detection of amyloid aggregates. Anal Chem 2020;92:2853−8.
[119] Springer T, Hemmerová E, Finocchiaro G, Kristofiková Z, Vyhnálek M, Homola J. Surface plasmon resonance biosensor for the detection of tau-amyloid β complex. Sensor Actuator B Chem 2020;316:128146.
[120] Patil PO, Pandey GR, Patil AG, Borse VB, Deshmukh PK, Patil DR, et al. Graphene-based nanocomposites for sensitivity enhancement of surface plasmon resonance sensor for biological and chemical sensing: a review. Biosens Bioelectron 2019;139:111324.
[121] Nangare S, Patil P. Chitosan mediated layer-by-layer assembly based graphene oxide decorated surface plasmon resonance biosensor for highly sensitive detection of β-amyloid. Int J Biol Macromol 2022;214:568−82.
[122] Khatril A, Punjabi N, Ghosh D, Maji SK, Mukherji S. Detection and differentiation of α-Synuclein monomer and fibril by chitosan film coated nanogold array on optical sensor platform. Sensor Actuator B Chem 2018;255:692−700.
[123] Kant R, Gupta BD. Fiber-optic SPR based acetylcholine biosensor using enzyme functionalized Ta_2O_5 nanoflakes for Alzheimer's diseasediagnosis. J Lightwave Technol 2018; 36:4018−24.
[124] Nu TTV, Tran NHT, Nam E, Nguyen TT, Yoon WJ, Cho S, et al. Blood-based immunoassay of tau proteins for early diagnosis of Alzheimer's disease using surface plasmon resonance fiber sensors. RSC Adv 2018;8:7855−62.
[125] Rezabakhsh A, Rahbarghazi R, Fathi F. Surface plasmon resonance biosensors for detection of Alzheimer's biomarkers; an effective step in early and accurate diagnosis. Biosens Bioelectron 2020;167:112511.
[126] Lyu S, Wu ZY, Shi XH, Wu Q. Optical fiber biosensors for protein detection: a review. Photonics-Basel 2022;9:987.
[127] Leitao C, Pereira SO, Marques C, Cennamo N, Zeni L, Shaimerdenova M, et al. Cost-effective fiber optic solutions for biosensing. Biosensors 2022;12:575.
[128] Jing JY, Liu K, Jiang JF, Xu TH, Wang S, Ma JY, et al. Performance improvement approaches for optical fiber SPR sensors and their sensing applications. Photon Res 2022;10: 126−47.
[129] Sai VVR, Kundu T, Mukherji S. Novel U-bent fiber optic probe for localized surface plasmon resonance based biosensor. Biosens Bioelectron 2009;24:2804−9.
[130] Yi XY, Xia YH, Ding BR, Wu L, Hu SQ, Wang ZX, et al. Dual-channel surface plasmon resonance for quantification of ApoE gene and genotype discrimination in unamplified genomic DNA extracts. ACS Sens 2018;3:2402−7.
[131] Kumaraswamy S, Tobias R. Label-free kinetic analysis of an antibody−antigen interaction using biolayer interferometry. In: Meyerkord CL, Fu H, editors. Protein-protein interactions: methods and applications. New York, NY: Springer New York; 2015. p. 165−82.
[132] Shah NB, Duncan TM. Bio-layer interferometry for measuring kinetics of protein-protein interactions and allosteric ligand effects. Jove-J Vis Exp 2014:e51383.
[133] Wilson JL, Scott IM, McMurry JL. Optical biosensing: kinetics of protein A-IGG binding using biolayer interferometry. Biochem Mol Biol Educ 2010;38:400−7.
[134] Ziu I, Laryea ET, Alashkar F, Wu CLG, Martic S. A dip-and-read optical aptasensor for detection of tau protein. Anal Bioanal Chem 2020;412:1193−201.
[135] Lausted C, Hu ZY, Hood L, Campbell CT. SPR imaging for high throughput, label-free interaction analysis. Comb Chem High Throughput Screen 2009;12:741−51.
[136] Gao HQ, Liu MZ, Zhao ZJ, Yang CX, Zhu L, Cai YN, et al. Diagnosis of mild cognitive impairment and Alzheimer's disease by the plasma and serum amyloid-beta 42 assay through highly sensitive peptoid nanosheet sensor. Acs Appl Mater Inter 2020;12:9693−700.
[137] Feng J, Siu VS, Roelke A, Mehta V, Rhieu SY, Palmore GTR, et al. Nanoscale plasmonic Iinterferometers for multispectral, high-throughput biochemical sensing. Nano Lett 2012; 12:602−9.
[138] Li DD, Odessey R, Li DF, Pacifici D. Plasmonic interferometers as TREM2 sensors for Alzheimer's disease. Biosensors 2021;11:217.
[139] Barve K, Singh U, Yadav P, Bhatia D. Carbon-based designer and programmable fluorescent quantum dots for targeted biological and biomedical applications. Mater Chem Front 2023;7:1781−802.
[140] Chen B, Wang F. Emerging frontiers of upconversion nanoparticles. Trends Chem 2020;2:427−39.
[141] Guo XR, Zhou LY, Liu XZ, Tan GJ, Yuan F, Nezamzadeh-Ejhieh A, et al. Fluorescence detection platform of metal-organic frameworks for biomarkers. Colloids Surf, B 2023; 229:113455.
[142] Liz-Marzán LM. Tailoring surface plasmons through the morphology and assembly of metal nanoparticles. Langmuir 2006;22:32−41.
[143] Loh KP, Bao QL, Eda G, Chhowalla M. Graphene oxide as a chemically tunable platform for optical applications. Nat Chem 2010;2:1015−24.
[144] Ma XY, Zhang TY, Wang XJ, Zhang TT, Zhang RY, Xu ZH, et al. Nanoparticles based on Prussian blue for biosensor applications: a review. ACS Appl Nano Mater 2023;6: 22568−93.
[145] Yang P, Zhang S, Chen XF, Liu XH, Wang Z, Li YW. Recent developments in polydopamine fluorescent nanomaterials. Mater Horiz 2020;7:746−61.
[146] Mo LT, Li J, Liu QL, Qiu LP, Tan WH. Nucleic acid-functionalized transition metal nanosheets for biosensing applications. Biosens Bioelectron 2017;89:201−11.
[147] Rocha-Santos TAP. Sensors and biosensors based on magnetic nanoparticles. Trac-Trend Anal Chem 2014;62:28−36.
[148] Phan LTT, Cho S. Fluorescent aptasensor and colorimetric aptablot for p-tau231 detection: toward early diagnosis of Alzheimer's disease. Biomedicines 2022;10:93.
[149] Xia N, Zhou BB, Huang NB, Jiang MS, Zhang JB, Liu L. Visual and fluorescent assays for selective detection of beta-amyloid oligomers based on the inner filter effect of gold nanoparticles on the fluorescence of CdTe quantum dots. Biosens Bioelectron 2016;85:625−32.
[150] Ren HX, Miao YB, Zhang YD. An aptamer based fluorometric assay for amyloid-β oligomers using a metal-organic framework of type Ru@MIL-101(Al) and enzyme-assisted recycling. Microchim Acta 2020;187:8.
[151] Jiang LF, Chen BC, Chen B, Li XJ, Liao HL, Huang HM, et al. Detection of Aβ oligomers based on magnetic-field-assisted separation of aptamer-functionalized Fe_3O_4 magnetic nanoparticles and BaYF:Yb,Er nanoparticles as upconversion fluorescence labels. Talanta 2017;170:350−7.
[152] de Arquer FPG, Talapin DV, Klimov VI, Arakawa Y, Bayer M, Sargent EH. Semiconductor quantum dots: technological progress and future challenges. Science 2021;373: eaaz8541.
[153] Zhu SJ, Song YB, Wang J, Wan H, Zhang Y, Ning Y, et al. Photoluminescence mechanism in graphene quantum dots: quantum confinement effect and surface/edge state. Nano Today 2017;13:10−4.
[154] Donegá CD. Synthesis and properties of colloidal heteronanocrystals. Chem Soc Rev 2011;40:1512−46.
[155] Empedocles SA, Bawendi MG. Quantum-confined Stark effect in single CdSe nanocrystallite quantum dots. Science 1997;278:2114−7.

[156] Chen L, Lin JW, Yi JQ, Weng QH, Zhou Y, Han ZZ, et al. A tyrosinase-induced fluorescence immunoassay for detection of tau protein using dopamine-functionalized CuInS/ZnS quantum dots. Anal Bioanal Chem 2019;411: 5277−85.
[157] Lu X, Hou X, Tang H, Yi X, Wang J. A high-quality CdSe/CdS/ZnS quantum-dot-based FRET aptasensor for the simultaneous detection of two different Alzheimer's disease core biomarkers. Nanomaterials 2022;12:14.
[158] Chen S, Yu YL, Wang JH. Inner filter effect-based fluorescent sensing systems: a review. Anal Chim Acta 2018;999: 13−26.
[159] Qian HF, Dong CQ, Weng JF, Ren JC. Facile one-pot synthesis of luminescent, water-soluble, and biocompatible glutathione-coated CdTe nanocrystals. Small 2006;2:747−51.
[160] Dabbousi BO, RodriguezViejo J, Mikulec FV, Heine JR, Mattoussi H, Ober R, et al. (CdSe)ZnS core-shell quantum dots: synthesis and characterization of a size series of highly luminescent nanocrystallites. J Phys Chem B 1997;101: 9463−75.
[161] Choudhury B, Dey M, Choudhury A. Shallow and deep trap emission and luminescence quenching of TiO_2 nanoparticles on Cu doping. Appl Nanosci 2014;4:499−506.
[162] Wang QB, Xu Y, Zhao XH, Chang Y, Liu Y, Jiang LJ, et al. A facile one-step in situ functionalization of quantum dots with preserved photoluminescence for bioconjugation. J Am Chem Soc 2007;129:6380−1.
[163] Sun YP, Zhou B, Lin Y, Wang W, Fernando KAS, Pathak P, et al. Quantum-sized carbon dots for bright and colorful photoluminescence. J Am Chem Soc 2006;128:7756−7.
[164] Li JY, Liu Y, Shu QW, Liang JM, Zhang F, Chen XP, et al. One-pot hydrothermal synthesis of carbon dots with efficient up- and down-converted photoluminescence for the sensitive detection of morin in a dual-readout assay. Langmuir 2017;33:1043−50.
[165] Tan S, Li S, Tang C, Bai X, Ran X, Qu Q, et al. A regenerable and reducing false-positive fluorescent switch for detection of β-amyloid1−42 oligomers. Talanta 2022;246:9.
[166] Liu C, Lu DK, You XR, Shi GY, Deng JJ, Zhou TS. Carbon dots sensitized lanthanide infinite coordination polymer nanoparticles: towards ratiometric fluorescent sensing of cerebrospinal Aβ monomer as a biomarker for Alzheimer's disease. Anal Chim Acta 2020;1105:147−54.
[167] Allendorf MD, Bauer CA, Bhakta RK, Houk RJT. Luminescent metal−organic frameworks. Chem Soc Rev 2009;38: 1330−52.
[168] Sun LD, Dong H, Zhang PZ, Yan CH. Upconversion of rare earth nanomaterials. Annu Rev Phys Chem 2015;66: 619−42.
[169] Ren HX, Zhong QL, Miao YB, Wen XW, Wu GY, Wang HL, et al. A label-free reusable aptasensor for Alzheimer's disease. Microchim Acta 2020;187:8.
[170] Wang XZ, Du J, Xiao NN, Zhang Y, Fei L, LaCoste JD, et al. Driving force to detect Alzheimer's disease biomarkers: application of a thioflavine T@Er-MOF ratiometric fluorescent sensor for smart detection of presenilin 1, amyloid β-protein and acetylcholine. Analyst 2020;145:4646−63.
[171] Fang WK, Liu L, Zhang LL, Liu D, Liu Y, Tang HW. Detection of amyloid β oligomers by a fluorescence ratio strategy based on optically trapped highly doped upconversion nanoparticles-SiO@metal-organic framework microspheres. Anal Chem 2021;93:12447−55.
[172] Ghosh D, Chattopadhyay N. Gold and silver nanoparticles based superquenching of fluorescence: a review. J Lumin 2015;160:223−32.
[173] Kong LN, Zhou XG, Shi GY, Yu YY. Molybdenum disulfide nanosheets-based fluorescent "off-to-on" probe for targeted monitoring and inhibition of β-amyloid oligomers. Analyst 2020;145:6369−77.
[174] Sun HY, Li DJ, Yue XJ, Hong R, Yang WH, Liu CR, et al. A review of transition metal dichalcogenides-based biosensors. Front Bioeng Biotechnol 2022;10:11.
[175] Chen WL, Gao G, Jin Y, Deng CY. A facile biosensor for Aβ40O based on fluorescence quenching of prussian blue nanoparticles. Talanta 2020;216:9.
[176] Liu L, Chang Y, Yu J, Jiang MS, Xia N. Two-in-one polydopamine nanospheres for fluorescent determination of beta-amyloid oligomers and inhibition of beta-amyloid aggregation. Sensor Actuator B Chem 2017;251:359−65.
[177] Yin YM, Chen GF, Gong L, Ge KZ, Pan WZ, Li N, et al. DNAzyme-powered three-dimensional DNA walker nanoprobe for detection amyloid β-peptide oligomer in living cells and in vivo. Anal Chem 2020;92:9247−56.
[178] Huang A, Zhang LN, Li WW, Ma ZY, Shuo S, Yao TM. Controlled fluorescence quenching by antibody-conjugated graphene oxide to measure tau protein. R Soc Open Sci 2018;5:171808.
[179] Zhao YN, Li X, Yang Y, Si SH, Deng CY, Wu HY. A simple aptasensor for Aβ40 oligomers based on tunable mismatched base pairs of dsDNA and graphene oxide. Biosens Bioelectron 2020;149:6.
[180] Saini M, Sadhu KK. Two instantaneous fluorogenic steps for detection of nanomolar amyloid beta monomer and its interaction with stoichiometric copper(II) ion. Sensor Actuator B Chem 2020;303:127086.
[181] Zhou J, Meng LC, Ye WR, Wang QL, Geng SZ, Sun C. A sensitive detection assay based on signal amplification technology for Alzheimer's disease's early biomarker in exosome. Anal Chim Acta 2018;1022:124−30.
[182] Dirks RM, Pierce NA. Triggered amplification by hybridization chain reaction. P Natl Acad Sci USA 2004;101: 15275−8.
[183] Fleischmann M, Hendra PJ, Mcquillan AJ. Raman-spectra of pyridine adsorbed at a silver electrode. Chem Phys Lett 1974;26:163−6.
[184] Moskovits M. Surface roughness and the enhanced intensity of Raman scattering by molecules adsorbed on metals. J Chem Phys 1978;69:4159−61.
[185] Kleinman SL, Frontiera RR, Henry AI, Dieringer JA, Van Duyne RP. Creating, characterizing, and controlling chemistry with SERS hot spots. Phys Chem Chem Phys 2013;15: 21−36.
[186] Pilot R, Signorini R, Durante C, Orian L, Bhamidipati M, Fabris L. A review on surface-enhanced Raman scattering. Biosensors 2019;9:57.
[187] Chou IH, Benford M, Beier HT, Coté GL, Wang M, Jing N, et al. Nanofluidic biosensing for β-amyloid detection using surface enhanced Raman spectroscopy. Nano Lett 2008;8: 1729−35.
[188] Wang GY, Hao CL, Ma W, Qu AH, Chen C, Xu J, et al. Chiral plasmonic triangular nanorings with SERS activity for ultrasensitive detection of amyloid proteins in Alzheimer's disease. Adv Mater 2021;33:7.
[189] Liu ZX, Ai J, Kumar P, You EM, Zhou X, Liu X, et al. Enantiomeric discrimination by surface-enhanced Raman scattering-chiral anisotropy of chiral nanostructured gold films. Angew Chem, Int Ed 2020;59:15226−31.
[190] Yu XK, Hayden EY, Wang P, Xia M, Liang O, Bai Y, et al. Ultrasensitive amyloid β-protein quantification with high dynamic range using a hybrid graphene-gold surface-enhanced Raman spectroscopy platform. J Raman Spectrosc 2020;51:432−41.
[191] Li ZY, Huang X, Lu G. Recent developments of flexible and transparent SERS substrates. J Mater Chem C 2020;8: 3956−69.
[192] Ling X, Xie LM, Fang Y, Xu H, Zhang HL, Kong J, et al. Can graphene be used as a substrate for Raman enhancement? Nano Lett 2010;10:553−61.
[193] El-Said WA, Kim TH, Yea CH, Kim H, Choi JW. Fabrication of gold nanoparticle modified ITO substrate to detect β-amyloid using surface-enhanced Raman scattering. J Nanosci Nanotechnol 2011;11:768−72.
[194] Yu D, Yin QL, Wang JW, Yang J, Chen ZM, Gao ZH, et al. SERS-based immunoassay enhanced with silver probe for

selective separation and detection of Alzheimer's disease biomarkers. Int J Nanomed 2021;16:1901−11.
[195] Yang SJ, Lee JU, Jeon MJ, Sim SJ. Highly sensitive surface-enhanced Raman scattering-based immunosensor incorporating half antibody-fragment for quantitative detection of Alzheimer's disease biomarker in blood. Anal Chim Acta 2022;1195:339445.
[196] Eremina OE, Yarenkov NR, Bikbaeva GI, Kapitanova OO, Samodelova M, Shekhovtsova TN, et al. Silver nanoparticle-based SERS sensors for sensitive detection of amyloid- β aggregates in biological fluids. Talanta 2024;266: 124970.
[197] Rochefort A, Wuest JD. Interaction of substituted aromatic compounds with graphene. Langmuir 2009;25:210−5.
[198] Manshina A, Povolotskiy A, Ivanova T, Kurochkin A, Tver'yanovich Y, Kim D, et al. CuCl2-based liquid electrolyte precursor for laser-induced metal deposition. Laser Phys Lett 2007;4:242−6.
[199] Arzhanukhina AI, Komova NS, Pavlov AM, Serdobintsev AA, Rusanova TY, Goryacheva IY. SERS assays based on electrospun nanofibers: preparation and analytical applications. Crit Rev Anal Chem 2023: 1−16.
[200] Jaiswal A, Naqvi TK, Dwivedi PK, Verma S. Single-platform, attomolar detection of multiple biomarkers by a flexible SERS sensor. Chem Asian J 2023;18:e202300441.
[201] Beier HT, Cowan CB, Chou IH, Pallikal J, Henry JE, Benford ME, et al. Application of surface-enhanced Raman spectroscopy for detection of beta amyloid using nanoshells. Plasmonics 2007;2:55−64.
[202] Xia Y, Padmanabhan P, Sarangapani S, Gulyás B, Matham MV. Bifunctional fluorescent/Raman nanoprobe for the early detection of amyloid. Sci Rep 2019;9:8497.
[203] Zhang X, Liu S, Song XL, Wang HW, Wang JF, Wang Y, et al. Robust and universal SERS sensing platform for multiplexed detection of Alzheimer's disease core biomarkers using PAapt-AuNPs conjugates. ACS Sens 2019;4: 2140−9.
[204] Pei H, Li F, Wan Y, Wei M, Liu HJ, Su Y, et al. Designed diblock oligonucleotide for thesynthesis of spatially Isolated and highly hybridizable functionalization of DNA-gold nanoparticle nanoconjugates. J Am Chem Soc 2012;134: 11876−9.
[205] Sharma H, Mutharasan R. Half antibody fragments improve biosensor sensitivity without loss of selectivity. Anal Chem 2013;85:2472−7.
[206] Yang JK, Hwang IJ, Cha MG, Kim HI, Yim D, Jeong DH, et al. Reaction kinetics-mediated control over silver nanogap shells as surface-enhanced Raman scattering nanoprobes for detection of Alzheimer's disease biomarkers. Small 2019;15:1900613.
[207] Zengin A, Tamer U, Caykara T. A SERS-based sandwich assay for ultrasensitive and selective detection of Alzheimer's tau protein. Biomacromolecules 2013;14:3001−9.
[208] Zhang LD, Cao K, Su Y, Hu S, Liang XH, Luo QM, et al. Colorimetric and surface-enhanced Raman scattering dual-mode magnetic immunosensor for ultrasensitive detection of blood phosphorylated tau in Alzheimer's disease. Biosens Bioelectron 2023;222:114935.
[209] Yu D, Yin QL, Wang JW, Yang J, Chen ZM, Gao ZH, et al. SERS-based immunoassay enhanced with silver probe for selective separation and detection of Alzheimer's disease biomarker. Int J Nanomed 2021;16:1901−11.
[210] Zhan YB, Fei RH, Lu Y, Wan Y, Wu XM, Dong J, et al. Ultrasensitive detection of multiple Alzheimer's disease biomarkers by SERS-LFA. Analyst 2022;147:4124−31.
[211] Sun JL, Shi ZL, Wang L, Zhang XY, Luo CS, Hua JY, et al. Construction of a microcavity-based microfluidic chip with simultaneous SERS quantification of dual biomarkers for early diagnosis of Alzheimer's disease. Talanta 2023;261: 124677.
[212] Ellington AD, Szostak JW. In vitro selection of RNA molecules that bind specific ligands. Nature 1990;346:818−22.
[213] Olsson B, Lautner R, Andreasson U, Öhrfelt A, Portelius E, Bjerke M, et al. CSF and blood biomarkers for the diagnosis of Alzheimer's disease: a systematic review and meta-analysis. Lancet Neurol 2016;15:673−84.
[214] Kim K, Lee CH, Park CB. Chemical sensing platforms for detecting trace-level Alzheimer's core biomarkers. Chem Soc Rev 2020;49:5446−72.
[215] Long S, Benoist C, Weidner W. World Alzheimer Report 2023: reducing dementia risk: never too early, never too late. London, UK: Alzheimer's Disease International; 2023.
[216] Brand AL, Lawler PE, Bollinger JG, Li Y, Schindler SE, Li M, et al. The performance of plasma amyloid beta measurements in identifying amyloid plaques in Alzheimer's disease: a literature review. Alzheimer's Res Ther 2022;14:195.
[217] O'Bryant SE, Gupta V, Henriksen K, Edwards M, Jeromin A, Lista S, et al. Guidelines for the standardization of pre-analytic variables for blood-based biomarker studies in Alzheimer's disease research. Alzheimers Dement 2015;11: 549−60.